AN ABSTRACT OF THE DISSERTATION OF

Eric J. Krebs for the degree of Doctor of Philosophy in Physics presented on August 26, 2015.

Title: Theory of Inhomogeneous Fluids

Abstract approved: _____

David J. Roundy

This dissertation reports on the computational physics research in the area of inhomogeneous fluids. I first discuss the theory background for this work beginning with water, which is important for the two published articles that are presented in this work (Chapters 5 and 6). Next, I give a brief overview of statistical associating fluid theory (SAFT), and discuss each free energy term and how it contributes to the SAFT free energy. I also give a short history of density functional theory (DFT) and discuss fundamental measure theory (FMT).

I then present a classical DFT for water along with simulation and comparisons with analytic data. Next, an improvement on the classical DFT for water is presented with a modified association free energy term. This improved DFT is compared to the previous theory and displays an overall improvement.

I present a soft sphere fluid theory based on soft fundamental measure theory with a Weeks-Chandler-Anderson (WCA) pair potential. I show that the results of

this theory are as good as a Barker-Henderson hard sphere fluid for low densities and a range of temperatures. I then derive the potential for a soft wall composed of WCA particles which was used to test the soft fluid theory.

Finally, I discuss a square well fluid theory that is currently incomplete. I present theory and up to our present work, display and discuss results, and mention possible problems.

Theory of Inhomogeneous Fluids

by

Eric J. Krebs

A DISSERTATION

submitted to

Oregon State University

in partial fulfillment of
the requirements for the
degree of

Doctor of Philosophy

Presented August 26, 2015
Commencement June 2016

Doctor of Philosophy dissertation of <u>Eric J. Krebs</u> presented on <u>August 26, 2015</u>.

APPROVED:

_____

Major Professor, representing Physics

_____

Chair of the Department of Physics

_____

Dean of the Graduate School

_____

Eric J. Krebs, Author

ACKNOWLEDGEMENTS

TABLE OF CONTENTS

LIST OF FIGURES

1 Introduction

My research at Oregon State University can be classified as research in liquid state theory, specifically inhomogeneous liquids. In total, I have contributed to two theory papers on water, a soft sphere theory that will be submitted for publication soon, and a square well fluid theory which is currently in progress. All of these projects have a number of aspects in common: they all rely on classical density functional theory (DFT) and they all require computational solutions. Monte-Carlo (MC) simulations, which are highly accurate, are utilized in two of the chapters as well.

The first few chapters give a brief background of the main theories used in this dissertation. I start by discussing motivations for studying water and recent notable research on water theories. I then describe statistical associating fluid theory (SAFT) and how each free energy term plays a role in SAFT. The last of these background chapters gives a brief history of density functional theory and how it led to its classical counterpart; Fundamental measure theory is also included as it is a classical DFT that is used throughout my research.

Chapters 5 and 6 are closely related theories of water which have been published. The purpose of studying water is to better understand its behaviour at nanoscale sizes. This can be beneficial in the study of biomolecular systems or for studying chemical reactions in aqueous solutions.

Chapter 5 presents a classical density functional theory for water by employing SAFT as the Helmholtz free energy term. A tuning parameter is introduced in the dispersion term of SAFT which changes the length scale over which dispersion is correlated. The model of water is then fit to experimental surface tension at ambient temperature along the water-vapor coexistence line.

In chapter 6, the association term of the previous chapter is modified using a more theoretically sound correlation at contact, and the tuning parameter introduced in Chapter 5 is adjusted for the new functional. Behavior of the improved DFT compared with the previous chapter's results are presented along with a Lennard-Jones approximation of a krypton atom solute. All comparisons show favorable results for the improved functional.

A majority of my effort was focused towards a soft sphere theory of fluids based on soft fundamental measure theory (SFMT). We initially chose a quadratic pair potential which could be used to solve for the weighted densities according to SFMT, but this pair potential proved troublesome. The theory became much more successful when we began using the Weeks-Chandler-Anderson (WCA) potential and made a few approximations to SFMT. Chapter 7 presents this theory and its results including comparison the Barker-Henderson hard sphere fluid. There is a soft wall potential that we use for testing the soft sphere theory which I have fully derived in Chapter 8.

Finally, Chapter 9 discusses my work on a square well fluid theory which is currently in development. After working on the theory portion and running simulation, it was found to have not-so-good agreement with MC simulation which led

us to realize that it may need to be modified in some way if our analytic derivations and code don't have errors.

2   Water

Water is considered an essential ingredient to sustain life, it is abundant on Earth, and is considered "the universal solvent." Water is the only substance on Earth that exists naturally in its solid, liquid, and gaseous form. Unlike most substances, when water transitions from liquid to solid state its density *decreases*, which is what allows ice to float in water. These are all interesting, but what about the more physical aspects of water?

Water has a rather high heat capacity, which can be thought of as its resistance to temperature change with respect to energy input. This is why living near a lake helps prevent large swings in temperature, thus regulating the climate of the surrounding area. Water also has about four hydrogen bond sites (two donor and two acceptor) near room temperature which allows interaction with other water molecules and solutes.

Water has a high surface tension which allows some small insects (and even lizards) to stand (or *run*) on bodies of water. Water ice has many different solid phases, ten of which are labeled in Figure 2.1.

Figure 2.1 shows a phase diagram of water. The green circle with the "E" in it at around 100 kPa and 300 Kelvin are typical conditions found on earth. Standard atmospheric pressure at the surface of earth is about 101 kPa, and we can see that moderate changes in temperature about "E" will give both solid and liquid states.
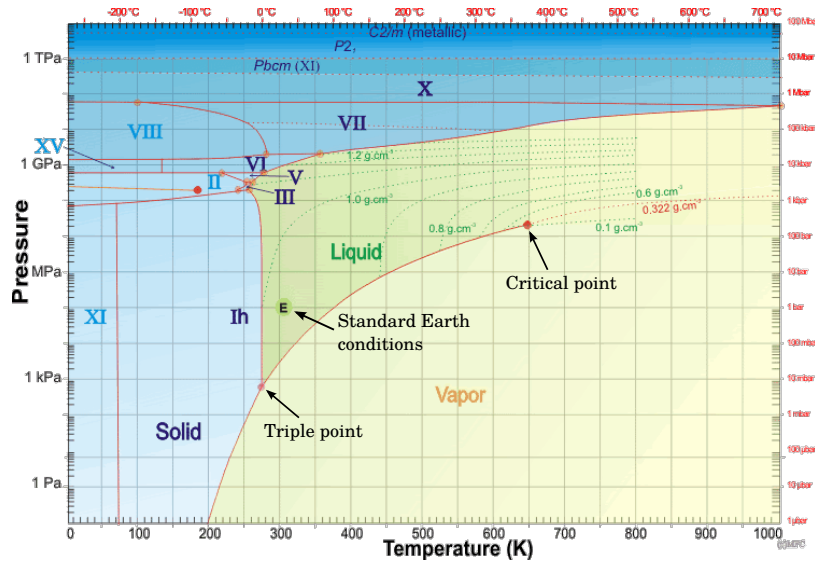
Figure 2.1: A phase diagram of water [1]. The circle marked "E" located in the liquid region at about 100 kPa of pressure and 300 K temperature is at typical conditions found on Earth. Both the triple point and critical point are labeled.

One thing of note that is not apparent in Figure 2.1 is behavior about the triple point (where all three states of water can exist simultaneously) and the solid-liquid transition line. The triple point of water is at about 273.16 Kelvin and 611.73 Pa, but at atmospheric pressure, freezing happens at the slightly lower 273.15 Kelvin. So what appears to be a straight solid-liquid transition line in Figure 2.1 is actually a line sloped to the left from the triple point. This gives the aforementioned fact that ice is less dense than liquid water. Phase diagrams for most other substances have the solid-liquid transition sloped to the right which gives a *higher* solid density.

Many studies of water have been performed using *ab initio* Molecular Dynamic (MD) simulations. This method considers interatomic and intra-atomic forces on

each atom and calculates the motion of each particle in the time domain. Although this can be considered a complete method to study fluids, it is not very ideal. MD simulations can typically follow only a few hundred water molecules per unit cell [6] and can take months to make calculations due to the small time steps required for accurate results.

Other methods to describe water have also met with undesirable results. An example is a continuum model of water using traditional density functional theories (DFT) that ignores dispersive forces such as van der Waals and instantaneous dipole forces. This particular model finds that ice melts at 120°C [7]. Even water models with a dispersive correction find that the melting point is still too high at 80°C [8]. Other corrections to this model make improvements at an increasingly expensive computational cost.

A good theory of water would produce useful properties, equation of state, correct behavior at interfaces, and would not be too computationally expensive. The theories presented in chapters 5 and 6 are positive steps toward these goals.

3 Statistical Associating Fluid Theory

Statistical associating fluid theory (SAFT) was formulated for describing homogeneous fluids and fluid mixtures that contain molecules which strongly interact with each other. It has been useful in scientific fields that deal with fluids such as chemical engineering. It has been used to study alcohols, electrolyte solutions, water, n-alkanes, and mixed systems . I will briefly describe each term in SAFT, and then look at each term individually in more detail.

3.1 SAFT terms

SAFT is an extension of Wertheim's thermodynamic perturbation theory [9–12] also called TPT1. SAFT is constructed to describe the contributions to the Helmholtz free energy of associating fluids. The total Helmholtz free energy for a fluid in SAFT is given by

$$F = F_{id} + F_{hs} + F_{disp} + F_{assoc} + F_{chain}. \tag{3.1}$$

F_{id} is the ideal gas energy term, F_{hs} is the energy contribution due to hard sphere repulsion, F_{disp} is the free energy due to dispersive interactions, F_{assoc} is the association energy due to hydrogen bonds, and F_{chain} is the energy due to chain formation in polymer fluids. Because F_{chain} does not play any important role in

the research presented in this dissertation, I will not be discussing it here.

3.2   Ideal gas contribution

Due to the nature of entropy and the Helmholtz free energy in statistical mechanics, the total free energy of a system can be broken up into an ideal gas free energy plus excess free energies. The ideal gas free energy has been known analytically for a long time, and it is the same result utilized in the SAFT ideal gas term.

Given an ideal gas made of N identical non-interacting particles with number density ρ and at temperature T,

$$F_{id} = Nk_BT \left(\ln \left(\Lambda^3 n \right) - 1 \right). \tag{3.2}$$

k_B is the Boltzmann constant, n is the density particle density and, Λ is the de Broglie thermal wavelength of a particle given by $\Lambda = \left(\frac{2\pi\hbar^2}{mk_BT} \right)^{1/2}$.

3.3   Hard sphere contribution

The hard sphere contribution to SAFT is the excess free energy due to a hard sphere repulsion between molecules, which does not allow any portion of two particle volumes to occupy the same space. Fundamental measure theory (FMT) [13] is a classical density functional theory for describing hard sphere systems which is used in this dissertation to determine the hard sphere contribution to SAFT. FMT will be discussed in more detail in Chapters 4 and 5.

3.4 Association term

The association free energy originates from short range interactions like hydrogen bonding within a fluid that reduces the overall energy but does not cause formation of polymer chains. Each molecule has an integer number of sites on its surface that "associate" with the sites on other molecules. For example, the theories presented in Chapters 5 and 6 have four association sites due to the nature of water. A graphical representation of this is given in Figure 3.1 where the associating spheres are show interacting (the green "glow") when the correct association sites are very close (donor/acceptor). The sphere immediately to the left shows a blue site in range of another blue site where there is no association. This represents a donor/donor or acceptor/acceptor site pair not interacting.

Since this is a statistical formulation, the key portion of the theory here deals with the fractional number of sites *not* bonded for any particular particle. The energy contribution due to association is

$$F_{assoc} = Mk_BT \sum_{i=1}^{M} \left[\ln X_i - \frac{X_i}{2} \right] + \frac{M}{2} \tag{3.3}$$

where M is the number of association sites on each molecule and X_i is the fraction of molecules not bonded at site i. For details of the dependence of X_i on temperature, density and the probability of spheres being in contact see Eq. 5.20 and Eq. 6.6.
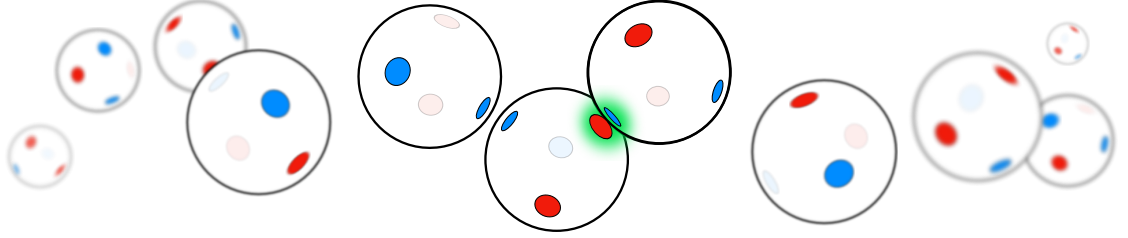
Figure 3.1: A representation of associating spheres. The three middle spheres are in close proximity, but only the green "glow" shows the association sites on the two spheres that are the correct types and close enough to interact.

3.5 Dispersive interactions

Dispersive forces, also known as London dispersion forces, are long range interactions between non-polar atoms or molecules. Interactions such as instantaneous dipole attraction is an example of such a force. Throughout this dissertation, the dispersion free energy has form

$$F_{disp} = \int \left(a_1(\mathbf{r}) + \beta a_2(\mathbf{r})\right) n(\mathbf{r})\mathrm{d}\mathbf{r}, \tag{3.4}$$

where the a_1 and a_2 terms are just the first two terms in a high temperature perturbation expansion and $\beta = 1/k_b T$. This can be seen by looking at the βa_2 term where each term would be of the order $\beta^{(i-1)}a_i$. If temperatures are high, β is small enough so that higher order terms can be dropped.

4 Classical Density Functional Theory

Classical thermodynamic theory has been very successful for ideal systems with little or no local fluctuation in density, temperature, pressure, and other measurable properties. These ideal systems are practically the definition of homogeneous, where the value of measurable quantities are the same throughout. Surely, though, only the most ideal systems are homogeneous, and any sort of interface such as the transition between water and air will causes density fluctuation. Since most systems have such interfaces and are not ideal, it would be very beneficial to have a theory that can describe these *in*homogeneous systems. If we have a theory for inhomogeneous systems, we can more accurately describe the world around us and make theoretical predictions which would be useful in a number of scientific fields including chemistry, biophysics, and chemical engineering. Classical density functional theory is a method for describing inhomogeneous systems of liquid and gases, which has superseded almost all other theories for such systems due to its simplicity and accuracy. Even though the theory had been around a while, it wasn't until computers became powerful enough that DFT could be fully realized.

4.1 Density and distribution

Before giving a full theory background, I should talk briefly about what a density distribution *is*. A general definition of density is an amount of "something" per

volume, and in density functional theory (DFT) we are referring to the *electron* density of a solid. But this density doesn't have to be a single homogeneous value of electrons per volume, it can be a density distribution. A distribution is a function which can take on different values associated with every location in space. What I'll refer to as the density $n(\mathbf{r})$ is a time averaged density distribution which describes the density of particles at each point, $\mathbf{r}$, in space.

4.2   Becoming a classical density functional theory

Density functional theory was formulated for dealing with systems with a large number of electrons based on a quantum mechanical description of the electron wave-function. The Thomas-Fermi model of electrons describes a system of free electrons as an "electron gas" where the electrons are *not* considered individually but as an electron density distribution that depends on position, $n(\mathbf{r})$.

In 1964, Hohenberg and Kohn [14] utilized this idea of electron density and came up with a variational formulation for the energy of a system in an external potential, $V_{ext}(\mathbf{r})$. The theorem states that the energy of a system can be a *functional* of density, $E[n(\mathbf{r})]$, and that the ground state energy of the system is determined by the correct density function for that energy. Any other density function returns a higher energy value;

$$E_0[n_0(\mathbf{r})] < E[n(\mathbf{r})] \text{ for } n_0(\mathbf{r}) \neq n(\mathbf{r}) \tag{4.1}$$

where E_0 and n_0 are the minimum energy and its density respectively. This turned a system of electrons into an energy minimization problem dependent on the density function $n(\mathbf{r})$. A drawback to this at the time was that it could only predict or approximate the ground state energy of the system at a temperature of $T = 0$ K.

The next year, 1965, Mermin took Hohenberg and Kohn's idea and applied it to a grand canonical ensemble at temperatures greater than zero [15]. Mermin's approach was to apply the ideas of classical thermodynamics and show that the grand potential can be written as

$$\Omega(T) = \min_{n(\mathbf{r})} \left\{ F[n(\mathbf{r}), T] + \int (V_{ext}(\mathbf{r}) - \mu) n(\mathbf{r}) d\mathbf{r} \right\}, \qquad (4.2)$$

where $F[n(\mathbf{r}), T]$ is the Helmholtz free energy, and μ is the chemical potential. A couple key points: $F[n(\mathbf{r}), T]$ is completely independent of $V_{ext}(\mathbf{r})$, and temperature is an input into the functional which can make predictions for $T > 0$ K. Even with these advances, the theory was still only meant to be applied to an electron gas. Over ten years later, Ebner *et al.* generalized this relation for application to systems comprised of atoms and molecules (not just electrons) [16]. Hence, we now have a *classical* density functional theory where $n(\mathbf{r})$ describes the time averaged number of atoms or molecules at each point in space.

4.3 Fundamental measure theory

Fundamental measure theory (FMT) is a successful implementation of classical density functional theory [13]. FMT describes hard sphere systems using weighted densities based on "fundamental measures" of hard spheres (i.e. the radius, mean radius of curvature, etc.). The weighted densities, n_i, take the form

$$n_i(\mathbf{r}) = \int n(\mathbf{r}')w_i(|\mathbf{r} - \mathbf{r}'|)d\mathbf{r}'. \tag{4.3}$$

where $n(\mathbf{r}')$ is the density distribution of hard spheres, w_i is a weight function, and $i = 0, 1, 2, 3, V1, V1$ refer to specific weighted densities. For an example on how these relate, the weight function w_3 describes the volume in which each sphere resides

$$w_3(\mathbf{r}) = \Theta(|\mathbf{r}| - R), \tag{4.4}$$

where R is the hard sphere radius. Then n_3 is the corresponding weighted density

$$n_3(\mathbf{r}) = \int n(\mathbf{r}')w_3(|\mathbf{r} - \mathbf{r}'|)d\mathbf{r}' \tag{4.5}$$

$$= \int n(\mathbf{r}')\Theta(|\mathbf{r} - \mathbf{r}'| - R)d\mathbf{r}'. \tag{4.6}$$

This weighted density shown graphically in Figure 4.1 is for a hard sphere fluid with $n(\mathbf{r}) = \sum \delta(\mathbf{r}_i)$.
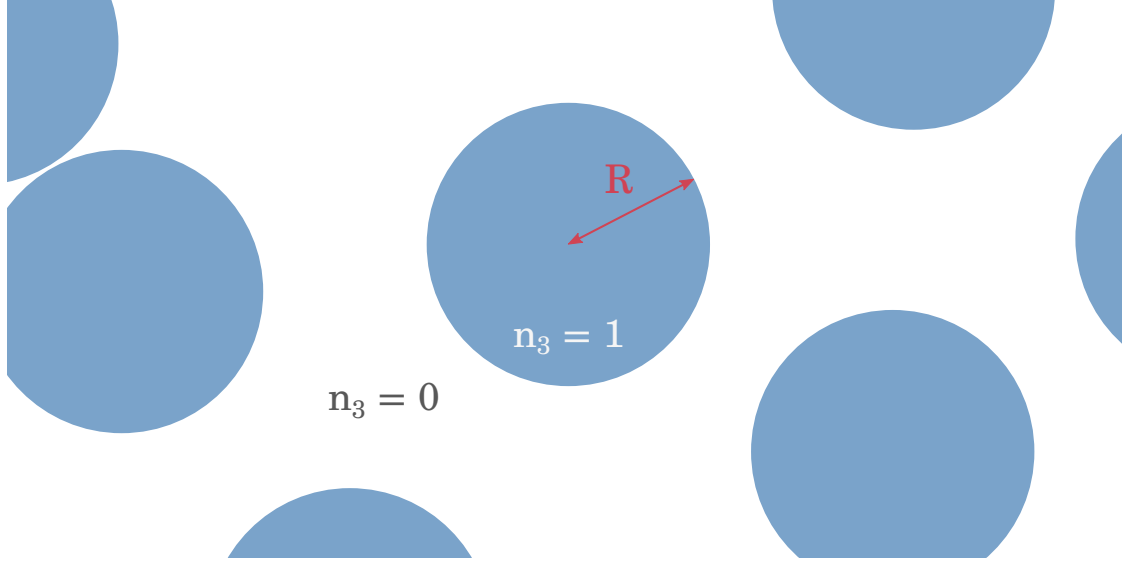
Figure 4.1: A two dimensional slice of n_3 for a hard sphere fluid with $n(\mathbf{r}) = \sum \delta(\mathbf{r}_i)$. The value of n_3 is 1 within the radius R of all hard spheres and 0 otherwise.

As another example, w_2 describes the surface of the spheres,

$$w_2(\mathbf{r}) = \delta(|\mathbf{r}| - R) \tag{4.7}$$

which the weighted density is shown graphically in Figure 4.2. The rest of the weighting functions $(w_0, w_1, \mathbf{w}_{1V}, \mathbf{w}_{2V})$ have simple dependencies on w_2, but it is unnecessary to show them here as they will appear in Chapter 7 and the weighted densities will appear in Chapter 5 of this dissertation.

How this relates to cDFT is in the excess free energy due to hard sphere repul-
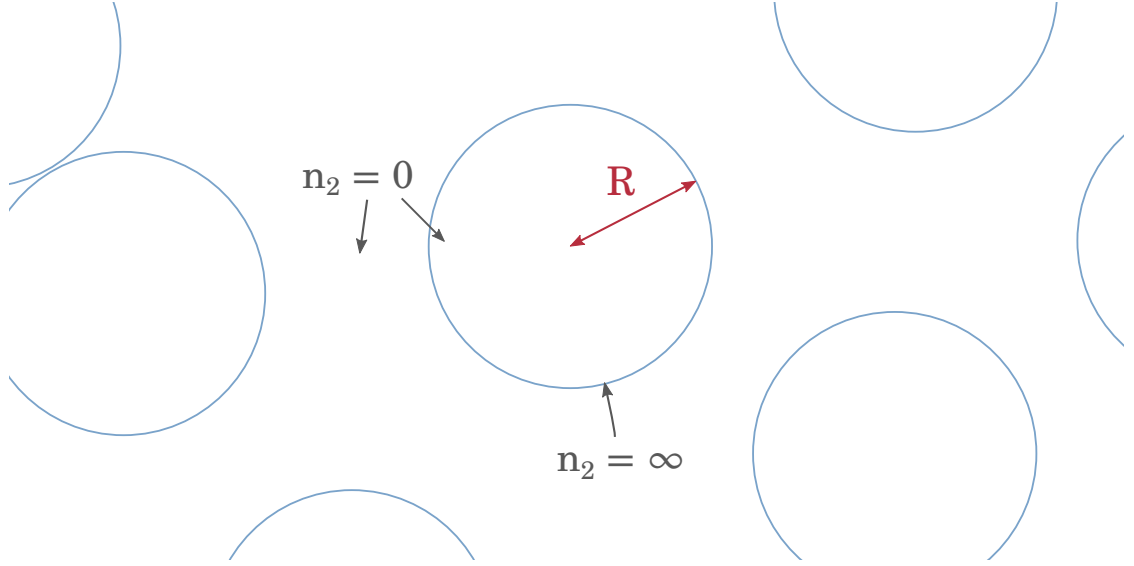
Figure 4.2: A two dimensional slice of n_2 for a hard sphere fluid with $n(\mathbf{r}) = \sum \delta(\mathbf{r}_i)$. Value of n_2 is ∞ at a the edge of the hard spheres and 0 otherwise.

sion:

$$F_{hs}[n] = k_B T \int \Bigg(\Phi_1\big(n_0(\mathbf{r}), n_3(\mathbf{r})\big)$$

$$+ \Phi_2\big(n_1(\mathbf{r}), n_2(\mathbf{r}), n_3(\mathbf{r}), \mathbf{n}_{V1}(\mathbf{r}), \mathbf{n}_{V2}(\mathbf{r})\big)$$

$$+ \Phi_3\big(n_2(\mathbf{r}), n_3(\mathbf{r}), \mathbf{n}_{V1}(\mathbf{r}), \mathbf{n}_{V2}(\mathbf{r})\big) \Bigg) d\mathbf{r} , \quad (4.8)$$

The Φs are a sort of energy densities (not exactly) that rely on the weighted densities. The total free energy for a fluid is the ideal gas contribution, F_{id}, plus whatever excess free energies exist in the system,

$$F = F_{id} + F_{ex}. \quad (4.9)$$

So for the hard sphere fluid, our total free energy is only the F_{id} and F_{hs} summed. This total free energy is then used in the grand potential (Equation 4.2) which can now be minimized.

5 A classical density-functional theory for water

The majority of the work in this chapter was performed by Jessica Hughes and became a paper [4] not too long after my help in this study. My main contributions to this work arose from simulating and plotting different configurations of rods in water. Specifically, I plotted density profiles for water near one, two, and four rod configurations. I found transition distances for the two and four rods systems (Figures 5.6 and 5.7), and compared values of density at contact from simulation to values analytically from the contact value theorem (Figure 5.4).

I contributed with other small tasks, but this paper mainly served as a stepping stone to my understanding of classical density functional theory, SAFT, FMT, and computational physics research.

5.1 Introduction

A large fraction of interesting chemistry—including all of molecular biology—takes place in aqueous solution. However, while quantum chemistry enables us to calculate the ground state energies of large molecules in vacuum, prediction of the free energy of even the smallest molecules in the presence of a solvent poses a continuing challenge due to the complex structure of a liquid and the computational cost of *ab initio* molecular dynamics [17, 18]. The current state-of-the art in *ab initio*

molecular dynamics is limited to a few hundred water molecules per unit cell [6]. On top of this, traditional density-functional theory (DFT) methods without the use of dispersion corrections strongly over-structure water, to the point that ice melts at over 120°C [7]! There has been a flurry of recent publications implicating van der Waals effects (i.e. dispersion corrections) as significant in reducing this over-structuring [19–22]. However, one particular study found that water modeled using a hybrid functional with dispersion corrections *still* has a melting point over 80°C [8]. It has also been found that the inclusion of nuclear quantum effects can provide similar improvements [23]. Each of these corrections imposes an additional computational burden on an approach that is already feasible for only a very small number of water molecules. A more efficient approach is needed in order to study nanoscale and larger solutes.

5.1.1   Classical density-functional theory

Numerous approaches have been developed to approximate the effect of water as a solvent in atomistic calculations. Each of these approaches gives an adequate description of some aspect of interactions with water, but none of them is adequate for describing *all* these interactions with an accuracy close to that attained by *ab initio* calculations. The theory of Lum, Chandler and Weeks (LCW) [24], for instance, can accurately describe the free energy cost of creating a cavity by placing a solute in water, but does not lend itself to extensions treating the strong interaction of water with hydrophilic solutes. Treatment of water as a continuum

dielectric with a cavity surrounding each solute can give accurate predictions for the energy of solvation of ions [25–30], but provides no information about the size of this cavity. In a physically consistent approach, the size of the cavity will naturally arise from a balance between the free energy required to create the cavity, the attraction between the water and the solute, and the steric repulsion which opens up the cavity in the first place.

One promising approach for an efficient continuum description of water is that of classical density-functional theory (DFT), which is an approach for evaluating the free energy and thermally averaged density of fluids in an arbitrary external potential [16]. The foundation of classical DFT is the Mermin theorem [15], which extends the Hohenberg-Kohn theorem [14] to non-zero temperature, stating that

$$\Omega(T) = \min_{n(\mathbf{r})} \left\{ F[n(\mathbf{r}), T] + \int (V_{ext}(\mathbf{r}) - \mu) n(\mathbf{r}) d\mathbf{r} \right\}, \tag{5.1}$$

where $\Omega(T)$ is the grand potential of a system in the external potential V_{ext} at temperature T, $n(\mathbf{r})$ is the density of atoms or molecules, μ is the chemical potential and $F[n(\mathbf{r}), T]$ is a universal free-energy functional for the fluid, which is independent of the external potential V_{ext}. Classical DFT is a natural framework for creating a more flexible theory of hydrophobicity that can readily describe interaction of water with arbitrary external potentials—such as potentials describing strong interactions with solutes or surfaces.

A number of exact properties are easily achieved in the density-functional framework, such as the contact-value theorem, which ensures a correct excess

chemical potential for small hard solutes. Much of the research on classical density-functional theory has focused on the hard-sphere fluid [13, 31–35], which has led to a number of sophisticated functionals, such as the fundamental-measure theory (FMT) functionals [13, 32–37]. These functionals are entirely expressed as an integral of local functions of a few convolutions of the density (fundamental measures) that can be efficiently computed. We will use the White Bear version of the FMT functional [36, 37]. This functional reduces to the Carnahan-Starling equation of state in the homogeneous limit, and it reproduces the exact free energy in the strongly-confined limit of a small cavity.

A number of classical density functionals have been developed for water [38–51], each of which captures some of the qualitative behavior of water. However, each of these functionals also fail to capture some of water's unique properties. For instance, the functional of Lischner *et al* [47] treats the surface tension correctly, but can only be used at room temperature, and thus captures none of the temperature-dependence of water. A functional by Chuev and Skolov [46] uses an ad hoc modification of FMT that can predict hydrophobic hydration near temperatures of 298 K, but does not produce a correct equation of state due to their method producing a high value for pressure. A number of classical density functionals have recently been produced that are based on Statistical Associating Fluid Theory (SAFT) [41–43, 45, 48, 50, 52–57]. These functionals are based on a perturbative thermodynamic expansion, and do reproduce the temperature-dependence of water's properties. We should give special mention to Sundararaman *et al* who recently introduced a classical density functional for water using a model in which

a water molecule is treated as a hard sphere attached to two tetrahedrally oriented hard spheres representing voids, or orientations in which a hydrogen bond may not be formed, with all attractive interactions being lumped into a single pair potential treated in a mean field approximation [51].

5.1.2   Statistical associating fluid theory

Statistical Associating Fluid Theory (SAFT) is a theory describing complex fluids in which hydrogen bonding plays a significant role [55,58]. SAFT is used to accurately model the equations of state of both pure fluids and mixtures over a wide range of temperatures and pressures. SAFT is based on Wertheim's first-order thermodynamic perturbation theory (TPT1) [9–12], which allows it to account for strong associative interactions between molecules.

The SAFT Helmholtz free energy is composed of five terms:

$$F = F_{id} + F_{hs} + F_{disp} + F_{assoc} + F_{chain}, \tag{5.2}$$

where the first three terms—ideal gas, hard-sphere repulsion and dispersion—encompass the *monomer* contribution to the free energy, the fourth is the *association* free energy, describing hydrogen bonds, and the final term is the chain formation energy for fluids that are chain polymers. While a number of formulations of SAFT have been published, we will focus on SAFT-VR [59], which was used by Clark *et al* to construct an optimal SAFT model for water [45]. All but
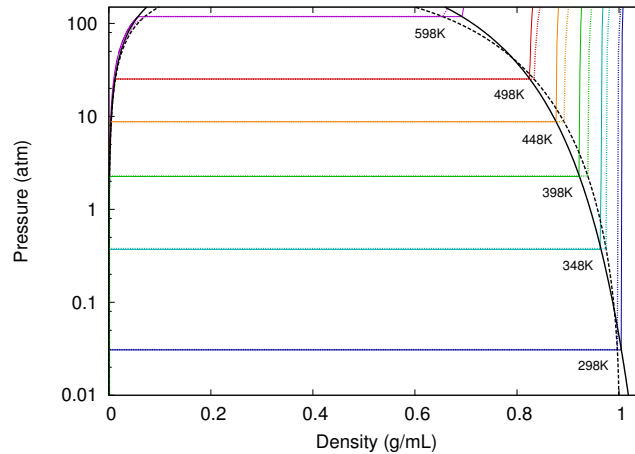
Figure 5.1: The pressure versus density for various temperatures, including experimental pressure data from NIST [2]. The solid colored lines indicate the computationally calculated pressure and the dotted colored lines are NIST data points. The solid and dotted black lines represent the theoretical and experimental coexistence curves.

one of the six empirical parameters used in the functional introduced in this paper are taken directly from this Clark *et al* paper. As an example of the power of this model, it predicts an enthalpy of vaporization at 100°C of ΔH_{vap}= 39.41 kJ/mol, compared with the experimental value ΔH_{vap}= 40.65 kJ/mol [2], with an error of only a few percent. We show a phase diagram for this optimal SAFT model for water in Figure 5.1, which demonstrates that its vapor pressure as a function of temperature is very accurate, while the liquid density shows larger discrepancies. The critical point is very poorly described, which is a common failing of models that are based on a mean-field expansion.

SAFT has been used to construct classical density functionals, which are often used to study the surface tension as a function of temperature [40–45,48–50,56,57].

Such functionals have qualitatively predicted the dependence of surface tension on temperature, but they also overestimate the surface tension by about 50%, and most SAFT-based functionals are unsuited for studying systems that have density variations on a molecular length scale due to the use of a local density approximation [41–43, 45, 49, 50, 57].

Functionals constructed using a local density approximation fail to satisfy the contact-value theorem, and therefore incorrectly model small hard solutes. The contact-value theorem relates the pressure on a hard surface to the contact density of the fluid at that surface:

$$p(\mathbf{r}_c) = n(\mathbf{r}_c)k_B T, \tag{5.3}$$

where $\mathbf{r}_c$ is the position at which a molecule is in contact with the hard surface, $n(\mathbf{r}_c)$ is the density at that point of contact, and $p(\mathbf{r}_c)$ is the pressure that the fluid exerts on the surface at the same point. This pressure is defined as a ratio of force to *solvent accessible surface* area. For a solute which excludes the solvent from an arbitrarily small volume, the contact density will be the same as the bulk density, and therefore we can integrate the above pressure to find that the excess chemical potential of a small hard solute is proportional to the solvent-excluded volume:

$$F = nk_B T V. \tag{5.4}$$

The contact-value theorem is violated by local classical density functionals such as those using a local density approximation or a square-gradient term, but is satisfied by non-local classical density functionals, such as those using a weighted-density

approach.

5.2 Theory and Methods

We construct a classical density functional for water, which reduces in the homogeneous limit to the optimal SAFT model for water found by Clark *et al.* The Helmholtz free energy is constructed using the first four terms from Equation 5.2: F_{id}, F_{hs}, F_{disp} and F_{assoc}. In the following sections, we will introduce the terms of this functional.

5.2.1 Ideal gas functional

The first term is the ideal gas free energy functional, which is purely local:

$$F_{id}[n] = k_B T \int n(\mathbf{x}) \left(\ln(n(\mathbf{x})\Lambda^3) - 1 \right) d\mathbf{x}, \qquad (5.5)$$

where $n(\mathbf{x})$ is the density of water molecules and Λ is the thermal wavelength $\Lambda = \left(\frac{2\pi\hbar^2}{mk_B T} \right)^{1/2}$. The ideal gas free energy functional on its own satisfies the contact value theorem and its limiting case of small solutes (Equations 5.3 and 5.4). These properties are retained by our total functional, since all the remaining terms are purely nonlocal.

5.2.2   Hard-sphere repulsion

We treat the hard-sphere repulsive interactions using the White Bear version of the Fundamental-Measure Theory (FMT) functional for the hard-sphere fluid [36, 37]. FMT functionals are expressed as the integral of the *fundamental measures* of a fluid, which provide local measures of quantities such as the packing fraction, density of spheres touching a given point and mean curvature. The hard-sphere excess free energy is written as:

$$F_{hs}[n] = k_B T \int (\Phi_1(\mathbf{x}) + \Phi_2(\mathbf{x}) + \Phi_3(\mathbf{x})) d\mathbf{x} \ , \tag{5.6}$$

with integrands

$$\Phi_1 = -n_0 \ln(1 - n_3) \tag{5.7}$$

$$\Phi_2 = \frac{n_1 n_2 - \mathbf{n}_{V1} \cdot \mathbf{n}_{V2}}{1 - n_3} \tag{5.8}$$

$$\Phi_3 = (n_2^3 - 3n_2 \mathbf{n}_{V2} \cdot \mathbf{n}_{V2}) \frac{n_3 + (1 - n_3)^2 \ln(1 - n_3)}{36\pi n_3^2 (1 - n_3)^2}, \tag{5.9}$$

where the fundamental measure densities are given by:

$$n_3(\mathbf{x}) = \int n(\mathbf{x}')\Theta(|\mathbf{x} - \mathbf{x}'| - R)d\mathbf{x}' \tag{5.10}$$

$$n_2(\mathbf{x}) = \int n(\mathbf{x}')\delta(|\mathbf{x} - \mathbf{x}'| - R)d\mathbf{x}' \tag{5.11}$$

$$\mathbf{n}_{V2} = \nabla n_3 \tag{5.12}$$

$$n_1 = \frac{n_2}{4\pi R} \tag{5.13}$$

$$\mathbf{n}_{V1} = \frac{\mathbf{n}_{V2}}{4\pi R} \tag{5.14}$$

$$n_0 = \frac{n_2}{4\pi R^2}. \tag{5.15}$$

The density n_3 is the packing fraction and n_0 is the average density at contact distance. For our functional for water, we use the hard-sphere diameter of 3.0342 Å, which was found to be optimal by Clark *et al.* [45]

5.2.3   Dispersion free energy

The dispersion free energy includes the van der Waals attraction and any orientation-independent interactions. We use a dispersion term based on the SAFT-VR approach [59], which has two free parameters (taken from Clark *et al* [45]): an interaction energy ϵ_d and a length scale $\lambda_d R$.

The SAFT-VR dispersion free energy has the form [59]

$$F_{\text{disp}}[n] = \int \left(a_1(\mathbf{x}) + \beta a_2(\mathbf{x})\right) n(\mathbf{x})d\mathbf{x}, \tag{5.16}$$

where a_1 and a_2 are the first two terms in a high-temperature perturbation expansion and $\beta = 1/k_B T$. The first term, a_1, is the mean-field dispersion interaction. The second term, a_2, describes the effect of fluctuations resulting from compression of the fluid due to the dispersion interaction itself, and is approximated using the local compressibility approximation (LCA), which assumes the energy fluctuation is simply related to the compressibility of a hard-sphere reference fluid [60].

The form of a_1 and a_2 for SAFT-VR is given in reference [59], expressed in terms of the packing fraction. In order to apply this form to an *inhomogeneous* density distribution, we construct an effective local packing fraction for dispersion η_d, given by a Gaussian convolution of the density:

$$\eta_d(\mathbf{x}) = \frac{1}{6\sqrt{\pi}\lambda_d^3 s_d^3} \int n(\mathbf{x}') \exp\left(-\frac{|\mathbf{x} - \mathbf{x}'|^2}{2(2\lambda_d s_d R)^2}\right) d\mathbf{x}'. \tag{5.17}$$

This effective packing fraction is used throughout the dispersion functional, and represents a packing fraction averaged over the effective range of the dispersive interaction. Here we have introduced an additional empirical parameter s_d which modifies the length scale over which the dispersion interaction is correlated.

5.2.4   Association free energy

The final attractive energy term is the association term, which accounts for hydrogen bonding. Hydrogen bonds are modeled as four attractive patches ("association sites") on the surface of the hard sphere. These four sites represent the two hydro-

gen bond donor sites, and two hydrogen bond acceptor sites. There is an attractive energy ϵ_a when two molecules are oriented such that the donor site of one overlaps with the acceptor site of the other. The volume over which this interaction occurs is κ_a, giving the association term in the free energy two empirical parameters that are fit to the experimental equation of state of water (again, taken from Clark *et al* [45]).

The association functional we use is a modified version of Yu and Wu [54], which includes the effects of density inhomogeneities in the contact value of the correlation function g_σ^{HS}, but is based on the SAFT-HS model, rather than the SAFT-VR model [59], which is used in the optimal SAFT parametrization for water of Clark *et al* [45]. Adapting Yu and Wu's association free energy to SAFT-VR simply involves the addition of a correction term in the correlation function (see Equation 5.22).

The association functional we use is constructed by using the density $n_0(\mathbf{x})$, which is the density of hard spheres touching a given point, in the standard SAFT-VR association energy [59]. The association free energy for our four-site model has the form

$$F_{\text{assoc}}[n] = 4k_BT \int n_0(\mathbf{x})\zeta(\mathbf{x}) \left(\ln X(\mathbf{x}) - \frac{X(\mathbf{x})}{2} + \frac{1}{2} \right) d\mathbf{x}, \qquad (5.18)$$

where the factor of 4 comes from the four association sites per molecule, the functional X is the fraction of association sites *not* hydrogen-bonded, and $\zeta(\mathbf{x})$ is a

dimensionless measure of the density inhomogeneity.

$$\zeta(\mathbf{x}) = 1 - \frac{\mathbf{n}_{V2} \cdot \mathbf{n}_{V2}}{n_2^2}.$$ (5.19)

The fraction X is determined by the quadratic equation

$$X(\mathbf{x}) = \frac{\sqrt{1 + 8n_0(\mathbf{x})\zeta(\mathbf{x})\Delta(\mathbf{x})} - 1}{4n_0(\mathbf{x})\zeta(\mathbf{x})\Delta(\mathbf{x})},$$ (5.20)

where the functional Δ is a measure of hydrogen-bonding probability, given by

$$\Delta(\mathbf{x}) = \kappa_a g_\sigma^{SW}(\mathbf{x}) \left(e^{\beta \epsilon_a} - 1\right)$$ (5.21)

$$g_\sigma^{SW}(\mathbf{x}) = g_\sigma^{HS}(\mathbf{x}) + \frac{1}{4}\beta \left(\frac{\partial a_1}{\partial \eta_d(\mathbf{x})} - \frac{\lambda_d}{3\eta_d}\frac{\partial a_1}{\partial \lambda_d}\right),$$ (5.22)

where g_σ^{SW} is the correlation function evaluated at contact for a hard-sphere fluid with a square-well dispersion potential, and a_1 and a_2 are the two terms in the dispersion free energy. The correlation function g_σ^{SW} is written as a perturbative correction to the hard-sphere fluid correlation function g_σ^{HS}, for which we use the functional of Yu and Wu [54]:

$$g_\sigma^{HS} = \frac{1}{1 - n_3} + \frac{R}{2}\frac{\zeta n_2}{(1 - n_3)^2} + \frac{R^2}{18}\frac{\zeta n_2^2}{(1 - n_3)^3}.$$ (5.23)
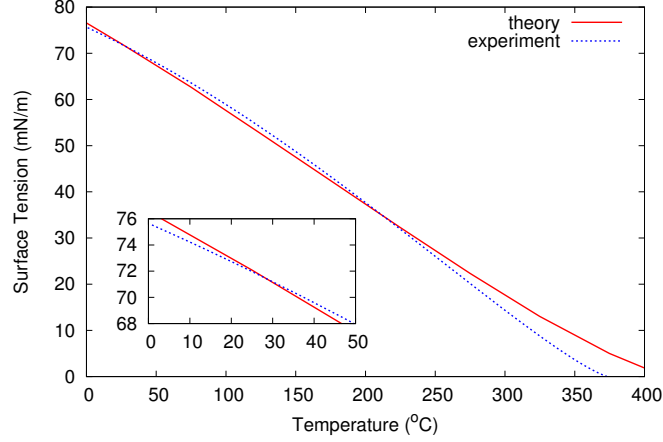
Figure 5.2: Comparison of Surface tension versus temperature for theoretical and experimental data. The experimental data is taken from NIST. [2] The length-scaling parameter s_d is fit so that the theoretical surface tension will match the experimental surface tension near room temperature.

5.2.5   Determining the empirical parameters

The majority of the empirical parameters used in our functional are taken from the paper of Clark *et al* on developing an optimal SAFT model for water [45]. This SAFT model contains five empirical parameters: the hard-sphere radius, an energy and length scale for the dispersion interaction, and an energy and length scale for the association interaction. In addition to the five empirical parameters of Clark *et al*, we add a single additional dimensionless parameter s_d—with a fitted value of 0.353—which determines the length scale over which the density is averaged when computing the dispersion free energy and its derivative. We determine this final parameter by fitting the computed surface tension to the experimental surface tension with the result shown in Figure 5.2. Because the SAFT model of Clark *et al*

overestimates the critical temperature—which is a common feature of SAFT-based functionals that do not explicitly treat the critical point—we cannot reasonably describe the surface tension at all temperatures, and choose to fit the surface tension at and around room temperature. We note here that we could have chosen to fit the surface tension with a square-gradient term in the free energy instead of adjusting the length scale for the dispersive attraction. This would result in a functional that violates the contact-value theorem which, among other problems, would fail to satisfy Equation 5.4 for the excess chemical potential of small solutes.

5.3   Results and discussion

5.3.1   One hydrophobic rod

We begin by studying a single hydrophobic rod immersed in water. In Figure 5.3 we show the excess chemical potential at room temperature, scaled by the solvent accessible surface area of the hard rod, plotted as a function of hard-rod radius. We define the hard-rods radius as the radius from which water is excluded. For rods with radius larger than 0.5 nm or so, this reaches a maximum value of 75 mN/m, which is slightly higher than macroscopic surface tension. In the limit of very large rods, this value will decrease and approach the macroscopic value. As seen in the inset of Fig. 5.3, for rods with very small radius (less than about 0.5 Å) the excess chemical potential is proportional to volume, satisfying Equation 5.4, which results from the contact-value theorem.

Figure 5.3: Excess chemical potential per area versus radius for a single hydrophobic rod immersed in water. This should have an asymptote equal to the surface tension at room temperature, and it agrees well with the surface tension in Figure 5.2. The inset for rods with a very small radius shows the linear relationship expected based on Equation 5.4.
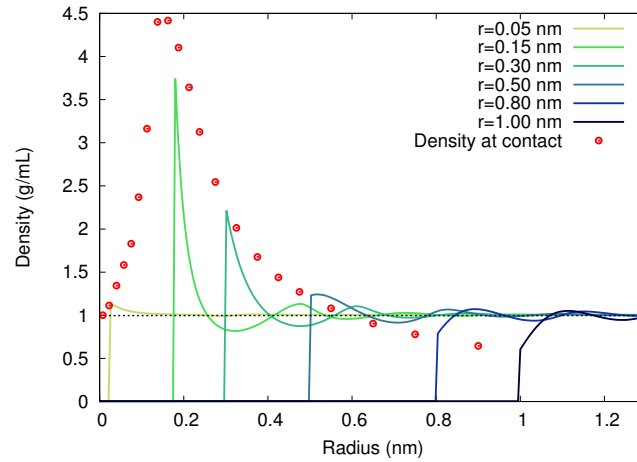
Figure 5.4: Density profiles for single rods of different radii. The dotted line represents the saturated liquid density and the points represent the expected contact density derived from the contact value theorem and calculated free energy data.

We show in Figure 5.4 density profiles for different radii rods, as well as the prediction for the contact value of the density as a function of rod radius, as computed from the excess chemical potentials plotted in Figure 5.3. The agreement between these curves confirms that our functional satisfies the contact-value theorem and that our minimization is well converged. As expected, as the radius of the rods becomes zero the contact density approaches the bulk density, and as the radius becomes large, the contact density will approach the vapor density.

5.3.2   Hydrophobic interaction of two rods

We now look at the more interesting problem of two parallel hard rods in water, separated by a distance d, as shown in Figure 5.5. At small separations there is only vapor between the rods, but as the rods are pulled apart, the vapor region expands until a critical separation is reached at which point liquid water fills the region between the rods. Figure 5.5 shows density profiles before and after this transition for rods of radius 0.6 nm. This critical separation for the transition to liquid depends on the radii of the rods, and is about 0.65 nm for the rods shown in Figure 5.5. The critical separation will be different for a system where there is attraction between the rods and water. At small separations, the shape of the water around the two rods makes them appear as one solid "stadium"-shaped object (a rectangle with semi-circles on both ends).

To understand this critical separation, we consider the free energy in the macro-
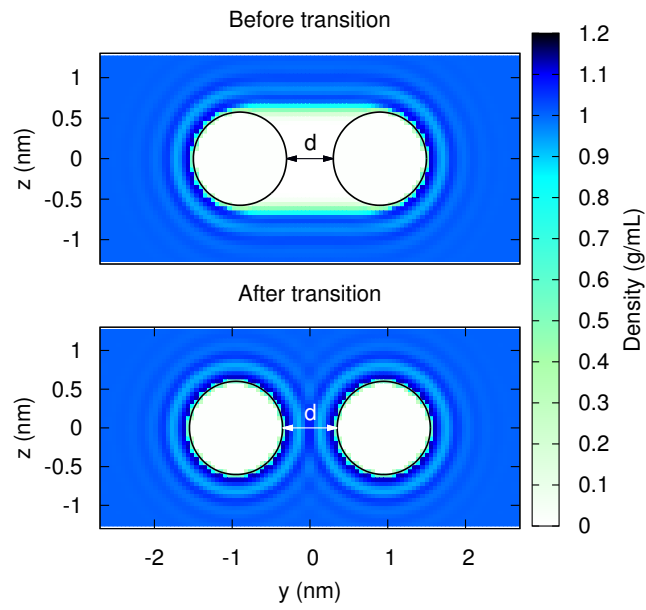
Figure 5.5: Density profiles illustrating the transition from vapor to liquid water between the rods. The radius is 0.6 nm, the top figure is at a separation of 0.6 nm and the bottom is 0.7 nm. Figure 5.6 shows the energy for these and other separations.

scopic limit, which is given by

$$F = \gamma A + pV. \tag{5.24}$$

The first term describes the surface energy and the second term is the work needed to create a cavity of volume V. Since the pressure term scales with volume, it can be neglected relative to the surface term provided the length scale is small compared with γ/p, which is around 20 μm, and is much larger than any of the systems we study. For micron-scale rods, the water on the sides of the 'stadium' configuration will bow inward between the rods and the density will reduce to vapor near the center point where the rods are closest to each other.

Starting from the surface energy term, we can calculate the free energy per length, which is equal to the circumference multiplied by the surface tension. Working out the circumference of the stadium-shape leads us to

$$F = (2\pi r + 4r + 2d)\gamma \tag{5.25}$$

where γ is the surface tension, r is the radius of the rods, and d is the separation between rods illustrated in Figure 5.5. The force per length is the derivative of the free energy with respect to the separation d, from which we conclude that the force per length is twice the surface tension.

We plot in Figure 5.6 the computed free energy of interaction per unit length from our classical density functional (solid lines), as a function of the separation d, along with the free energy predicted by our simple macroscopic model (dashed
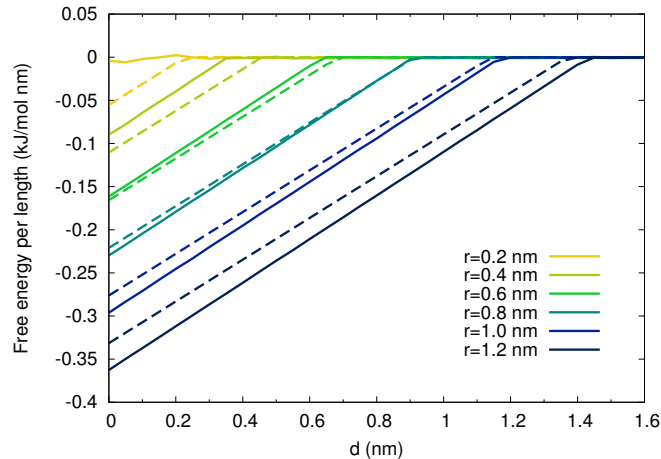
Figure 5.6: Free energy of interaction (also known as the potential of mean force) versus separation for two hydrophobic rods ranging in radius from 0.2 nm to 1.2 nm. All were arbitrarily offset to zero at large separations for ease of comparison. The transition corresponds to the phase change from vapor to liquid between the rods as pictured in the density profiles in Figure 5.5.

lines). The models agree very well on the force between the two rods at close separations, and have reasonable agreement as to the critical separation for rods greater than 0.5 nm in radius.

Walther *et al* [61] studied the interactions between two carbon nanotubes, which are geometrically similar to our hydrophobic rods, using molecular dynamics with the SPC model for water. Their simulations used nanotubes of diameter 1.25 nm and separations ranging from about 0.3 nm to 1.5 nm. In agreement with our findings for two purely hydrophobic rods, Walther *et al* find that in the absence of Lennard-Jones attraction between carbon and oxygen, there is a drying transition at a distance comparable to the diameter of the nanotube. In contrast to this, when the attraction between nanotubes and water is turned on, they find
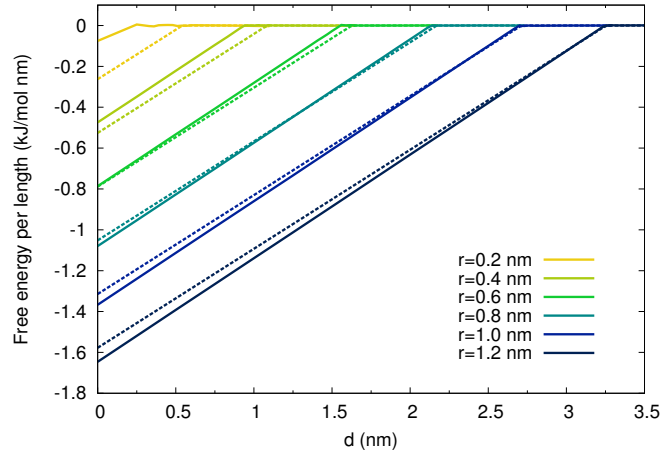
Figure 5.7: Free energy of interaction versus separation for four hydrophobic rods ranging in radius from 0.2 nm to 1.2 nm. All were arbitrarily offset to zero at large separations. The transition corresponds to the phase change from vapor to liquid between the rods as pictured in the density profiles in Figure 5.8.

that the drying transition occurs at much shorter distances, comparable to the diameter of water.

5.3.3   Hydrophobic interactions of four rods

We go on to study four parallel hard rods, as examined by Lum, Chandler and Weeks in their classic paper on hydrophobicity at small and large length scales [24]. As in the case of two rods—and as predicted by Lum *et al*—we observe a drying transition, as seen the density plot shown in Figure 5.8. In Figure 5.7, we plot the free energy of interaction together with the macroscopic approximation, and find good agreement for rods larger than 0.5 nm in radius. This free energy plot is qualitatively similar to that predicted by the LCW theory [24], with the difference
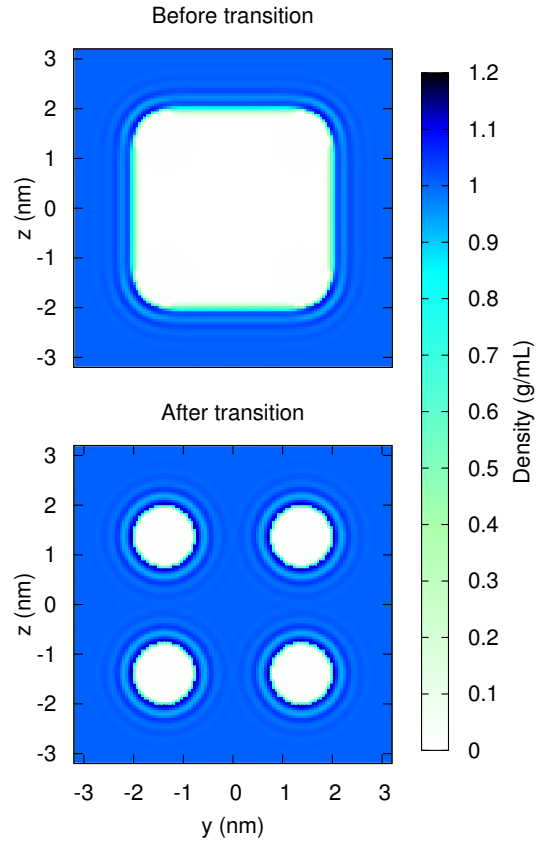
Figure 5.8: Density profiles illustrating the transition from vapor to liquid water between four rods. The radius is 0.6 nm, the top figure is at a separation of 1.53 nm and the bottom is 1.56 nm. Figure 5.7 shows the energy for these and other separations.
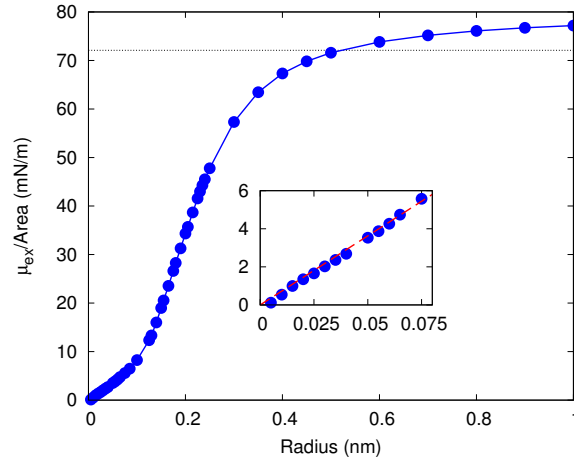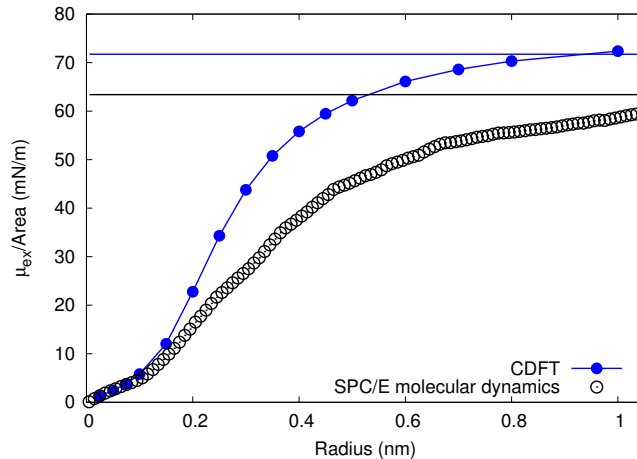
Figure 5.9: Excess chemical potential per area versus radius for a single hydrophobic sphere immersed in water. This should have an asymptote equal to the surface tension at room temperature, and it agrees well with the surface tension in Figure 5.2. Results from a simulation of SPC/E water [3] are shown as circles. The horizontal lines show the experimental and SPC/E macroscopic surface tension for water at standard atmospheric temperature and pressure.

that we find no significant barrier to the association of four rods.

5.3.4 Hydration energy of hard-sphere solutes

A common model of hydrophobic solutes is the hard-sphere solute, which is the simplest possible solute, and serves as a test case for understanding of hydrophobic solutes in water [62]. As in the single rod, we begin by examining the ratio of the excess chemical potential of the cavity system to the solvent accessible surface area (Figure 5.9). This effective surface tension surpasses the macroscopic surface tension at a radius of almost 1 nm, and at large radius will drop to the macroscopic
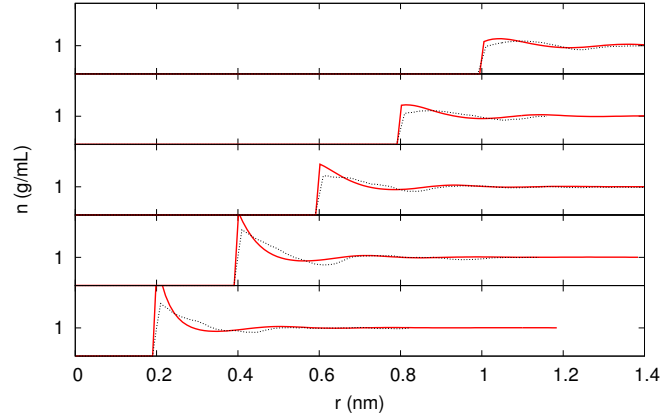
Figure 5.10: Density profiles around hard-sphere solutes of different radii. Predictions from our classical density-functional theory are in solid red, while the dotted line shows the result of a molecular dynamics simulation of SPC/E water [3].

value. As with the single rod, we see the analytically correct behavior in the limit of small solutes. For comparison, we plot the free energy calculated using a molecular dynamics simulation of SPC/E water [3]. The agreement is quite good, apart from the issue that the SPC/E model for water significantly underestimates the macroscopic surface tension of water at room temperature [63].

Figure 5.10 shows the density profile for several hard sphere radii, plotted together with the results of the same SPC/E molecular dynamics simulation shown in Figure 5.9 [3]. The agreement with simulation is quite reasonable. The largest disagreement involves the density at contact, which according to the contact value theorem cannot agree, since the free energies do not agree.

5.4 Conclusion

We have developed a classical density functional for water that combines SAFT with the fundamental-measure theory for hard spheres, using one additional empirical parameter beyond those in the SAFT equation of state, which is used to match the experimental surface tension. This functional does *not* make a local density approximation, and therefore correctly models water at both small and large length scales. In addition, like all FMT functionals, this functional is expressed entirely in terms of convolutions of the density, which makes it efficient to compute and minimize.

We apply this functional to the case of hard hydrophobic rods and spheres in water. For systems of two or four hydrophobic rods surrounded by water, we see a transition from a vapor-filled state a liquid-filled state. A simple model treatment for the critical separation for this transition works well for rods with diameters larger than 1 nm. In the case of spherical solutes, we find good agreement with SPC/E simulations.

6 An Improved classical density-functional theory for water

This chapter is a slightly modified version of a published paper [64] which utilizes results from another paper [65] (created by our research group) on the research in Chapter 5. All modifications to the published paper in this chapter are conversions from citations (Hughes *et al.* [4]) to chapter and equation reference from this dissertation. All figures have been left in their original form where the legends label Hughes *et al.* in comparison to "this work." The captions are modified to clarify that Hughes *et al.* is a reference to Chapter 5 from this dissertation.

6.1 Introduction

Water, the universal solvent, is of critical practical importance, and a continuum description of water is in high demand for a solvation model. A number of recent attempts to develop improved solvation models for water have built on the approach of classical density functional theory (DFT) [66–72]. Classical DFT is based on a description of a fluid written as a free energy functional of the density distribution. There are two general approaches used to construct a classical DFT for water. The first is to choose a convenient functional form which is then fit to properties of the bulk liquid at a given temperature and pressure [47,66–72]. Using this approach, it is possible to construct a functional that reproduces the exact second-order response function of the liquid under the fitted conditions. However,

this class of functional will be less accurate at other temperatures or pressures—
and in the inhomogeneous scenarios in which solvation models are applied. The
second approach is to construct a functional by applying liquid-state theory to a
model system, and then fit the model to experimental data such as the equation
of state [4, 41–46, 48–51].

A widely used family of models used in the development of classical density
functionals is based on Statistical Associating Fluid Theory (SAFT) [58]. SAFT is
a theory based on a model of hard spheres with weak dispersion interactions and
hydrogen-bonding association sites, which has been used to accurately model the
equations of state of both pure fluids and mixtures over a wide range of tempera-
tures and pressures [55, 73]. The association contribution to the free energy uses
Wertheim's first-order thermodynamic perturbation theory to describe an associat-
ing fluid as hard-spheres with strong associative interactions at specific sites on the
surface of each sphere [9–12]. These association sites have an attractive interaction
at contact, and rely on the hard-sphere pair distribution function at contact g_σ^{HS}
in order to determine the extent of association. While this function is known for
the homogeneous hard-sphere fluid, it must be approximated for inhomogeneous
systems, such as occur at liquid interfaces.

In another paper from my research group, the pair distribution function at con-
tact in various inhomogeneous configurations [65] was examined by Schulte *et al.*
Schulte *et al.* tested the accuracy of existing approximations for the pair distribu-
tion function at contact [54, 56], and derived a significantly improved approxima-
tion for the averaged distribution function at contact. In this paper we apply this

improved g_σ^{HS} to the SAFT-based classical density functional for water developed in Chapter 5. This functional was constructed to reduce in the homogeneous limit to the 4-site optimal SAFT model for water developed by Clark *et al.* [45]. The DFT of Chapter 5 uses the association free energy functional of Yu and Wu [54], which is based on a g_σ^{HS} that has since found to be inaccurate [65]. In this paper, we will examine the result of using the improved functional for g_σ^{HS} developed in Chapter 5 to construct an association free energy functional.

6.2 Method

The classical density functional for water of Chapter 5 consists of four terms:

$$F[n(\mathbf{r})] = F_{\text{ideal}}[n(\mathbf{r})] + F_{\text{HS}}[n(\mathbf{r})] + F_{\text{disp}}[n(\mathbf{r})] + F_{\text{assoc}}[n(\mathbf{r})] \qquad (6.1)$$

where F_{ideal} is the ideal gas free energy and F_{HS} is the hard-sphere excess free energy, for which we use the White Bear functional [36]. F_{disp} is the free energy contribution due to the square-well dispersion interaction; this term contains one empirical parameter, s_d, which is used to fit the surface tension of water near one atmosphere. Finally, F_{assoc} is the free energy contribution due to association, which is the term that we examine in this paper.

6.2.1 Dispersion

The dispersion term in the free energy includes the van der Waals attraction and any orientation-independent interactions. Following Chapter 5, we use a dispersion term based on the SAFT-VR approach [59], which has two free parameters (taken from Clark *et al* [45]): an interaction energy ϵ_d and a length scale $\lambda_d R$.

The SAFT-VR dispersion free energy has the form [59]

$$F_{\text{disp}}[n] = \int \left(a_1(\mathbf{x}) + \beta a_2(\mathbf{x}) \right) n(\mathbf{x}) d\mathbf{x} \qquad (6.2)$$

where a_1 and a_2 are the first two terms in a high-temperature perturbation expansion and $\beta = 1/k_B T$. The first term, a_1, is the mean-field dispersion interaction. The second term, a_2, describes the effect of fluctuations resulting from compression of the fluid due to the dispersion interaction itself, and is approximated using the local compressibility approximation (LCA), which assumes the energy fluctuation is simply related to the compressibility of a hard-sphere reference fluid [60].

The form of a_1 and a_2 for SAFT-VR is given in reference [59], expressed in terms of the packing fraction. In order to apply this form to an *inhomogeneous* density distribution, we construct an effective local packing fraction for dispersion η_d, given by a Gaussian convolution of the density:

$$\eta_d(\mathbf{x}) = \frac{1}{6\sqrt{\pi}\lambda_d^3 s_d^3} \int n(\mathbf{x}') \exp\left(-\frac{|\mathbf{x} - \mathbf{x}'|^2}{2(2\lambda_d s_d R)^2} \right) d\mathbf{x}'. \qquad (6.3)$$

This effective packing fraction is used throughout the dispersion functional, and
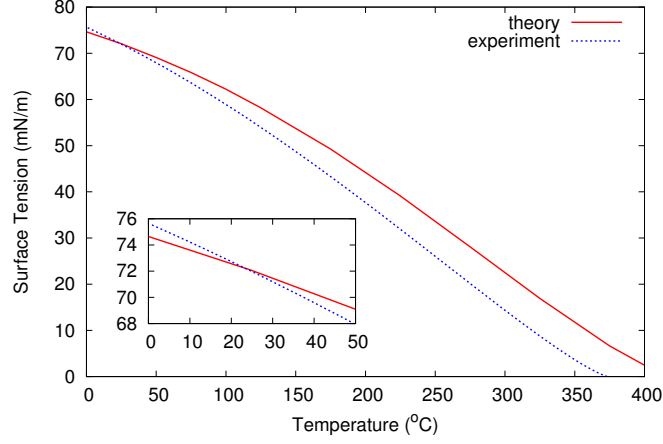
Figure 6.1: Comparison of Surface tension versus temperature for theoretical and experimental data. The experimental data is taken from NIST [2]. The length-scaling parameter s_d is fit so that the theoretical surface tension will match the experimental surface tension near room temperature.

represents a packing fraction averaged over the effective range of the dispersive interaction. Eq. 6.3 contains an additional empirical parameter s_d introduced in Chapter 5, which modifies the length scale over which the dispersion interaction is correlated.

6.2.2 Association

The association free energy for our four-site model has the form:

$$F_{\text{assoc}}[n] = k_B T \int n_{\text{site}}(\mathbf{x}) \left(\ln X(\mathbf{x}) - \frac{X(\mathbf{x})}{2} + \frac{1}{2} \right) d\mathbf{x} \qquad (6.4)$$

where $n_{\text{site}}(\mathbf{r})$ is the density of bonding sites at position $\mathbf{r}$:

$$n_{\text{site}}(\mathbf{r}) = \begin{cases} 4n(\mathbf{r}) & \text{this work} \\ \\ 4n_0(\mathbf{r})\zeta(\mathbf{r}) & \text{Hughes } \textit{et al.} \text{ (Eq. 5.18 this dissertation)} \end{cases} \tag{6.5}$$

where the factor of four comes from the four hydrogen bond sites, the fundamental measure $n_0(\mathbf{r})$ is the average density contacting point $\mathbf{r}$, and $\zeta(\mathbf{x})$ is a dimensionless measure of the density inhomogeneity from Yu and Wu [54]. The functional $X(\mathbf{r})$ is the fraction of association sites *not* hydrogen-bonded, which is determined for our 4-site model by the quadratic equation

$$X(\mathbf{x}) = \frac{\sqrt{1 + 2n'_{\text{site}}(\mathbf{r})\kappa_a g_\sigma^{SW}(\mathbf{x})\left(e^{\beta\epsilon_a} - 1\right)} - 1}{n'_{\text{site}}(\mathbf{r})\kappa_a g_\sigma^{SW}(\mathbf{x})\left(e^{\beta\epsilon_a} - 1\right)}, \tag{6.6}$$

where

$$n'_{\text{site}}(\mathbf{r}) = \begin{cases} \frac{4}{\pi\sigma^2} \int n(\mathbf{r}')\delta(\sigma - |\mathbf{r} - \mathbf{r}'|)d\mathbf{r}' & \text{this work} \\ \\ 4n_0(\mathbf{r})\zeta(\mathbf{r}) & \text{Hughes } \textit{et al.} \text{ (Eq. 5.20 this dissertation)} \end{cases} \tag{6.7}$$

is the density of bonding sites that could bond to the sites $n_{\text{site}}(\mathbf{r})$, and

$$g_\sigma^{SW}(\mathbf{x}) = g_\sigma^{HS}(\mathbf{x}) + \frac{1}{4}\beta\left(\frac{\partial a_1}{\partial\eta_d(\mathbf{x})} - \frac{\lambda_d}{3\eta_d}\frac{\partial a_1}{\partial\lambda_d}\right), \tag{6.8}$$

where g_σ^{HS} is the correlation function evaluated at contact for a hard-sphere fluid with a square-well dispersion potential, and a_1 and a_2 are the two terms in the dispersion free energy defined above (Eq. 6.2). The radial distribution function of the square-well fluid g_σ^{SW} is written as a perturbative correction to the hard-sphere radial distribution function g_σ^{HS}. The functional of Chapter 5 uses the g_σ^{HS} from Yu and Wu [54]. In this Chapter, we use the g_σ^{HS} derived by Schulte *et al.* [65].

As in Chapter 5, we use Clark's five empirical parameters, and fit the calculated surface tension to experimental surface tension at ambient conditions by tuning the parameter s_d, which adjusts the length-scale of the average density used for the dispersion interaction. With the improved association term, we find these agree when s_d is 0.454, which is an increase from the value of 0.353 found in Chapter 5. In order to explore further the change made by the improved association term, we compared the new functional with that of Chapter 5 for the two hydrophobic cases of the hard rod and the hard spherical solute.

6.3   Results

We will first discuss the case of a single hard rod immersed in water. Figure 6.2 shows the density profile of water near a rod with radius 1 Å. The density computed using the functional of this paper is qualitatively similar to that from Chapter 5, with a comparable density at contact—consistent with having made only a moderate change in the free energy. The first density peak near the surface is higher than that from Chapter 5, and the peak has a kink at the top. This reflects the
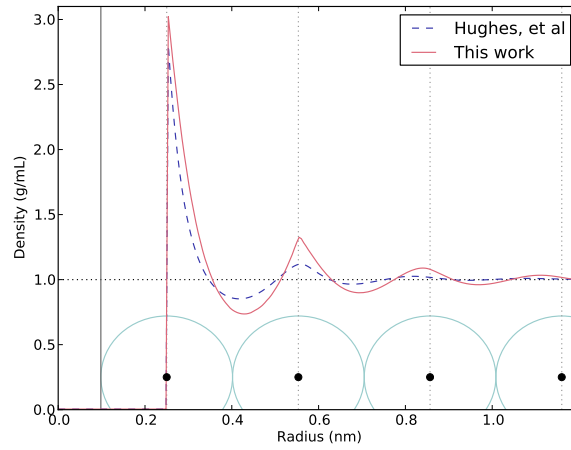
Figure 6.2: Density profiles for a water around a single hard rod of radius 0.1 nm. The solid red profile is from the functional developed in this paper and the dashed blue profile is the result from Hughes *et al.* [4] (Chapter 5 in this dissertation). For scale, under the profiles is a cartoon of a string of hard spheres touching in one dimension. The horizontal black dotted line is the bulk density for water and the vertical line on the left at 0.1 nm represents the rod wall.
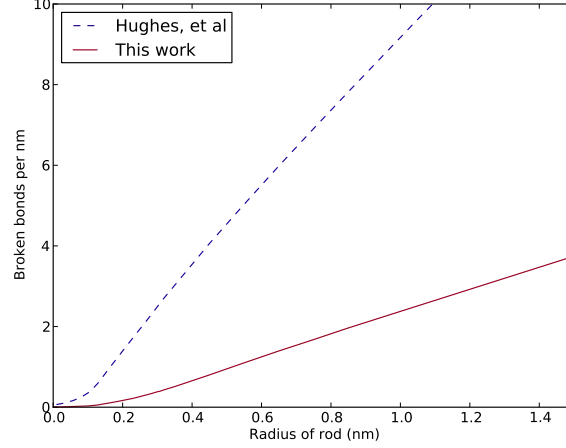
Figure 6.3: Broken hydrogen bonds per nanometer for hard rods immeresed in water. The solid red line uses the functional developed in this paper while the dashed blue line uses the functional from Hughes *et al.* [4] (Chapter 5 in this dissertation). For large enough rods, the graph increases linearly for both functionals.

improved accuracy of the g_σ^{HS} from Chapter 5, since beyond the first peak water molecules are unable to touch—or hydrogen bond to—molecules at the surface of the hard rod. This is illustrated under the profiles in Figure 6.2 by a cartoon of adjacent hard spheres that are increasingly distant from the hard rod surface.

In addition to the density, we examine the number of hydrogen bonds which are broken due to the presence of a hard rod. We define this quantity as

$$N_{\text{broken HB}} = 2 \int (X(\mathbf{r}) - X_{\text{bulk}})n_{\text{site}}(\mathbf{r})d\mathbf{r} \tag{6.9}$$

where $X_{\text{bulk}} = 0.13$ is the fraction of unbonded association sites in the bulk. The factor of 2 is chosen to account for the four association sites per molecule, and the

fact that each broken hydrogen bond must be represented twice—once for each of the molecules involved. In Fig. 6.3 we show the number of hydrogen bonds broken by a hard rod per nanometer length, as predicted by the functional of Chapter 5 (dashed line) and this work (solid line), as a function of the radius of the hard rod. In each case in the limit of large rods, the number of broken bonds is proportional to the surface area. At every radius, the functional of Chapter 5 predicts approximately four times as many broken hydrogen bonds as the improved functional.

A common test case for studying hydrophobic solutes in water is the hard-sphere solute. Figure 6.4 shows results for the number of broken hydrogen bonds caused by a hard-sphere solute, as a function of the solute radius. As in Fig. 6.3, the number of broken bonds scales with surface area for large solutes, and the number of broken bonds is about four times smaller than the number from the functional of Chapter 5. For solutes smaller than 3 Å in radius, there is less than a tenth of a hydrogen bond broken. This is consistent with the well-known fact that small solutes (unlike large solutes) do not disrupt the hydrogen-bonding network of water [74].

Finally, in order to compare with experimental results, we examined the hydration of Krypton. To describe the interaction of water with krypton, we use a Lennard-Jones potential with values $\epsilon = .9518$ kJ/mol and $\sigma = 3.42$ Å calculated using the Lorentz-Berthelot mixing rules and the Lennard-Jones parameters for water from SPC/E calculations [75]. Figure 6.5 shows the krypton-oxygen partial radial distribution function $g_{Kr-O}(r)$, which gives the relative probability density
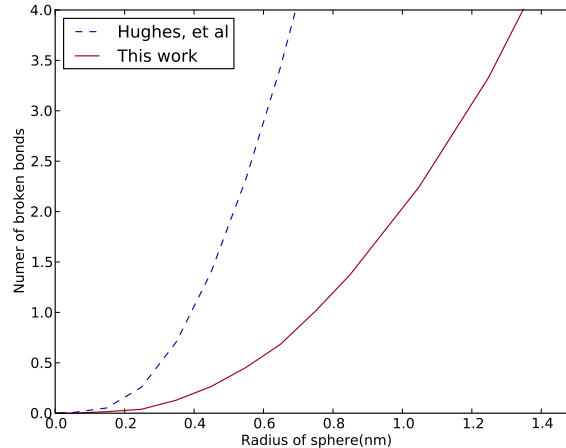
Figure 6.4: Broken hydrogen bonds for hard spheres immeresed in water. The solid red line uses our the functional developd in this paper while the dashed blue line is from Hughes *et al.* [4] (Chapter 5 in this dissertation).

that an oxygen atom resides at a distance r from a krypton atom centered at the origin. We present theoretical curves computed using both this work and the functional of Chapter 5, which we compare with experimental data from extended x-ray absorption fine structure spectroscopy (EXAFS) [5]. The new functional shows improved agreement with experiment in the height and position of the first maximum as well as the hight and position of the first minimum in $g_{Kr-O}(r)$ when compared with that of Chapter 5

6.4   Conclusion

We have modified the classical DFT for water developed in Chapter 5 by with the more accurate radial distribution function at contact developed by Schulte *et*
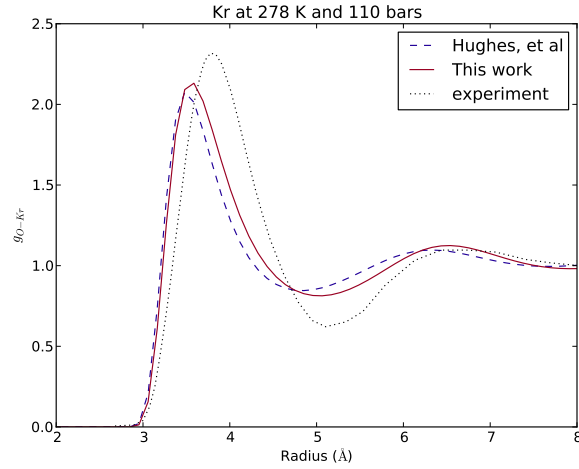
Figure 6.5: The Kr-O partial radial distribution function at low temperature (5°C) and high pressure (110 bar) in the limit of low concentration of krypton in water. The dashed blue line is computed using using the functional from Hughes *et al.* [4] (Chapter 5 from this dissertation), the solid red line is this work, and the black dotted line is from experiment [5].

al. [65], which affects the predicted hydrogen bonding between water molecules. We found that while this modification has a relatively mild effect on the free energy and density profiles, it predicts fewer broken hydrogen bonds around hard hydrophobic solutes and at aqueous interfaces. The improved functional does indeed show better agreement with experiment when used to compute the partial radial distribution function of a krypton atom dissolved in water.

7 A soft sphere fluid functional based on Soft Fundamental Measure Theory

7.1 Introduction

The idea of liquids as composed of hard spheres dates back over two millenia [76]. In the 20th century, we came to understand atoms as inherently soft, but it was shown that their repulsion could still be accurately described using a hard-sphere model, provided the radius is chosen to be temperature dependent [77–79]. These works cemented the hard-sphere model as the reference system of choice for the theory of liquids [45, 59, 80]. One reason for the wide use of the hard-sphere fluid hard sphere fluid as a reference system is that it is widely studied and well understood, not only for the homogeneous fluid [81], but also in the more challenging case of the inhomogeneous fluid [13, 33, 36]. However, the hard-sphere fluid remains a non-physical model, which is also numerically inconvenient in its use of delta functions.

Fundamental Measure Theory (FMT) is a classical density functional theory for the free energy of the hard-sphere fluid developed by Rosenfeld [13]. Due to its combination of computational efficiency with accuracy, FMT has since been used as the basis for a wide variety of classical density functionals [4,64,82–84], including those in the previous two chapters. In 1999, Schmidt introduced *Soft* Fundamental

Measure Theory (SFMT) [85], which directly treats soft repulsive potentials in a framework based on the highly successful FMT developed by Rosenfeld [13]. SFMT has been used to describe the behavior of a star polymer in solution [86–89], as well as repulsive potentials applicable to atoms [89, 90].

In this paper, we will apply SFMT to study the Weeks-Chandler-Anderson (WCA) repulsive potential [91]. This potential reproduces the repulsive force of a Lennard-Jones interaction, which makes it an ideal model for interatomic repulsion. Mathematically, the WCA pair potential is given by

$$
V_{\text{wca}}(r) = \begin{cases} 4\epsilon \left[\left(\frac{\sigma}{r} \right)^{12} - \left(\frac{\sigma}{r} \right)^{6} \right] + \epsilon, & 0 < r < 2R \\ 0, & \text{otherwise.} \end{cases} \tag{7.1}
$$

where ϵ and σ are the usual Lennard-Jones parameters and R is a single sphere radius which is related by $\sigma = 2^{5/6}R$. In this paper we will used the dimensionless reduced density $n^* \equiv n\sigma^3$ and reduced temperature $T^* \equiv k_B T/\epsilon$.

7.2 Methods

7.2.1 Soft Fundamental Measure Theory

Soft fundamental measure theory (SFMT) is a generalization of FMT to soft interactions developed by Schmidt [85]. Like Rosenfeld's FMT [13], the free energy is written as an integral of functions of a set of weighted densities known as *fun-*

damental measures:

$$A_{HS}[n] = k_B T \int \left(\Phi_1(\mathbf{r}) + \Phi_2(\mathbf{r}) + \Phi_3(\mathbf{r}) \right) d\mathbf{r} \,, \tag{7.2}$$

with integrands

$$\Phi_1 = -n_0 \ln \left(1 - n_3 \right) \tag{7.3}$$

$$\Phi_2 = \frac{n_1 n_2 - \mathbf{n}_{V1} \cdot \mathbf{n}_{V2}}{1 - n_3} \tag{7.4}$$

$$\Phi_3 = \frac{n_2^3 - 3 n_2 \mathbf{n}_{V2} \cdot \mathbf{n}_{V2}^2}{24\pi (1 - n_3)^2} \tag{7.5}$$

which is derived from dimensional crossover from the exact free energy in the zero-dimensional cavity limit [85]. The fundamental measures

$$n_i(\mathbf{r}) = \int n(\mathbf{r}') w_i(|\mathbf{r} - \mathbf{r}'|) d\mathbf{r}' \tag{7.6}$$

are defined as convolutions with weight functions similar to those of hard-sphere FMT. Like hard-sphere fundamental measures, the new weight functions are constructed so as to deconvolve the Mayer function,

$$f(r) = \exp(-\beta V(r)) - 1 \tag{7.7}$$

where $\beta = 1/k_B T$. The weighting functions are related by

$$\mathbf{w}_{V2} = w_2 \frac{\mathbf{r}}{r} \qquad\qquad \mathbf{w}_{V1} = w_1 \frac{\mathbf{r}}{r} \qquad\qquad (7.8)$$

$$w_1 = \frac{w_2}{4\pi R} \qquad\qquad w_0 = \frac{w_2}{4\pi R^2} \qquad\qquad (7.9)$$

$$w_3(r) = \int_r^\infty w_2(r')dr', \qquad\qquad (7.10)$$

where it is helpful to note that the integral in Eq. 7.10 is a one-dimensional integral over radius.

Furthermore, Schmidt proves that SFMT produces the exact functional in the low-density limit, provided the weighting function that defines n_2 is related to the slope of the Mayer function by a convolution with itself

$$\frac{df(r)}{dr} = \int dr' w_2(r')w_2(r - r'), \qquad\qquad (7.11)$$

with the other weighting functions given by the equations above [90]. We note that these equations are satisfied by traditional hard-sphere FMT as well as SFMT, for the same reason: they are needed in order to ensure the correct low-density behavior. Equation 7.11 is the challenge point for SFMT: deconvolving the Mayer f function for a realistic potential is challenging, which has limited the number of applications of this theory to simple liquids.

There are two options for constructing a theory directly using SFMT: either one must choose a pair potential and deconvolve the Mayer function to solve for w_2—which is difficult—or one can construct a w_2 and solve for the pair potential that

weighting function represents. In the original papers introducing SFMT, Schmidt exclusively studied models analytically in which the potential is proportional to temperature [85, 90]. While this proportionality is correct for purely entropic interactions, such as the star polymer in solution studied in several papers [85], this assumption is not applicable to energetic interactions such as dominate repulsion between molecules. Here we will discuss the *error function model* (or *erf model*) introduced by Schmidt in Ref. 90.

The erf model corresponds to a Gaussian form for the weighting function w_2 The weight function for the erf model is

$$w_2(r) = \frac{1}{\Xi\sqrt{\pi}} e^{-\frac{(r-\alpha/2)^2}{\Xi^2}} \tag{7.12}$$

where Ξ and α are parameters with dimensions of length. This choice for w_2 results in a form containing an error function for the w_3 weighting function, the Mayer f function, and the pair potential:

$$w_3(r) = \tfrac{1}{2}\left(1 - \operatorname{erf}\left(\frac{r-\alpha/2}{\Xi}\right)\right) \tag{7.13}$$

$$f(r) = \tfrac{1}{2}\left(\operatorname{erf}\left(\frac{r-\alpha}{\Xi}\right) - 1\right) \tag{7.14}$$

$$V_{\mathrm{erf}}(r) = -kT\ln\left[\tfrac{1}{2}\left(\operatorname{erf}\left(\frac{r-\alpha}{\Xi}\right) + 1\right)\right]. \tag{7.15}$$

The erf potential is shown in Fig. 7.1, and the first derivative of the Mayer f function corresponding to this potential is shown in Fig. 7.2. Sadly, as is evident from Eq. 7.15, this simple functional relationship only holds for one chosen temperature.

At other temperatures, the same potential leads to an entirely different form for f and w_2, which is not analytically tractable.

7.2.2 Barker-Henderson hard sphere

Another approach to account for the temperature dependence of realistic fluids is Barker-Henderson's approach [78]. This theory takes any general repulsive pair potential, $V(r)$, and creates a hard sphere reference fluid with a temperature dependent diameter and higher order repulsive terms. The hard sphere diameter is

$$d = \int_0^\infty \left(1 - e^{-\beta V(r)}\right) dr. \tag{7.16}$$

We utilize this variable diameter to create a White Bear [36] hard sphere DFT and compare its behavior with the soft sphere DFT we construct in this paper.

We use the White Bear version of the Fundamental-Measure Theory (FMT) functional [36], which describes the excess free energy of an inhomogeneous hard-sphere fluid. The White Bear functional reduces to the Carnahan-Starling free energy for homogeneous systems, and has been found to be accurate under a wide range of inhomogeneous configurations.

$$A_{HS}[n] = k_B T \int \left(\Phi_1(\mathbf{r}) + \Phi_2(\mathbf{r}) + \Phi_3(\mathbf{r})\right) d\mathbf{r} , \tag{7.17}$$

with integrands

$$\Phi_1 = -n_0 \ln(1 - n_3) \tag{7.18}$$

$$\Phi_2 = \frac{n_1 n_2 - \mathbf{n}_{V1} \cdot \mathbf{n}_{V2}}{1 - n_3} \tag{7.19}$$

$$\Phi_3 = (n_2^3 - 3n_2 \mathbf{n}_{V2} \cdot \mathbf{n}_{V2}) \frac{n_3 + (1 - n_3)^2 \ln(1 - n_3)}{36\pi n_3^2 (1 - n_3)^2}, \tag{7.20}$$

using the weighted density

$$n_2(\mathbf{r}) = \int n(\mathbf{r}') w_2(|\mathbf{r} - \mathbf{r}'| - R) d\mathbf{r}' \tag{7.21}$$

$$= \int n(\mathbf{r}') \delta(|\mathbf{r} - \mathbf{r}'| - R) d\mathbf{r}' \tag{7.22}$$

where the remaining weighted densities are given by Eqs. 7.6 through 7.10.

7.2.3   Soft FMT for the WCA fluid

Our approach to model the WCA fluid is to approximate the WCA potential by using the erf potential with temperature-dependent parameters. We select the parameters Ξ and α to match the value and derivative of $V_{\mathrm{erf}}(r)$ and $V_{\mathrm{wca}}(r)$ at the distance α, corresponding to the maximum slope of the Mayer f function. In essence, this is similar to the Barker-Henderson approach, in which a hard-sphere potential with temperature-dependent diameter is used to model a soft repulsive fluid.

We begin by equating the values of the potentials at distance α, which tells us
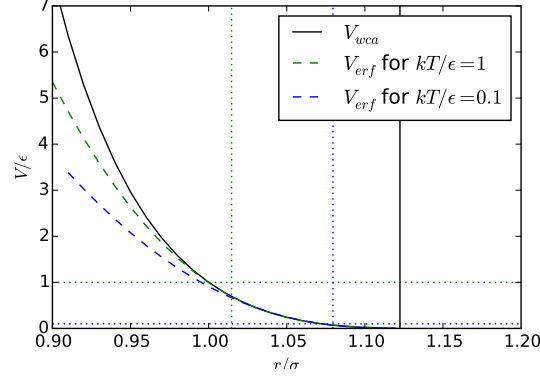
Figure 7.1: The WCA potential, and approximations to this potential constructed for two different temperatures.

that the α parameter must be given by

$$\alpha = \sigma \left(\frac{2}{1 + \sqrt{\frac{k_B T}{\epsilon} \ln 2}} \right)^{\frac{1}{6}}. \tag{7.23}$$

The alpha parameter roughly measures the length-scale of the interaction, and like the Barker-Henderson diameter, decreases with increasing temperature. Finally, equating the slope of both potentials at $r = \alpha$ yields the other parameter

$$\Xi = \frac{\alpha}{6\sqrt{\pi} \left(\sqrt{\frac{\epsilon}{k_B T} \ln 2} + \ln 2 \right)}, \tag{7.24}$$

which is a measure of the effective softness of the interaction, and increases with the temperature. We show the resulting approximation for the potential in Figures 7.1 for two different temperatures. We see the temperature dependence of
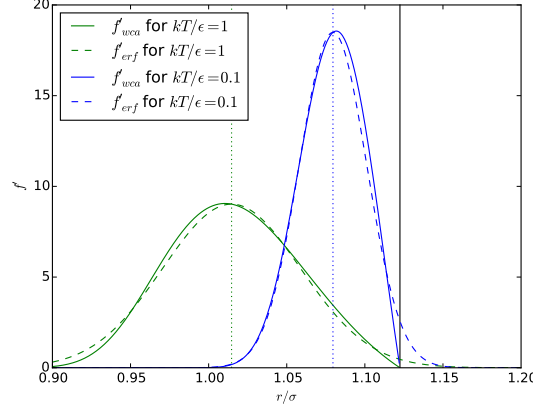
Figure 7.2: The derivative of the Mayer f function from the WCA potential, and the convolution of the fitted Gaussian w_2 with itself at two different temperatures. According to Eq. 7.11 these should be identical in order to accurately reproduce the low-density behavior of the fluid.

the approximation in comparison to the WCA potential, with the approximation at higher temperatures being more accurate for smaller differences. Vertical dotted lines show the values of α at which V_{erf} and V_{wca} are matched, a solid black vertical line represents the distance at which the WCA force goes to zero, and the horizontal dotted lines illustrate the two temperatures. At both temperatures, the largest deviations are seen at very small distances, and thus very high potential energies.

Figure 7.2 compares the derivative of the Mayer f function corresponding to the WCA pair potential with convolution of the the fitted Gaussian w_2 from Eq. 7.12 with itself, as in Eq. 7.11. The two vertical dotted lines show the α where the potential functions have been matched, and the the solid vertical line shows where the WCA force, and potential, and thus f'_{wca}, goes to zero. The erf result extends

slightly past the cutoff at which f'_{wca} vanishes for both temperatures, but does quickly go to zero. At lower lower temperatures w_2 and f' are more peaked and approach the cutoff, as the system approaches hard-sphere behavior in which these functions are Dirac δ functions.

In Appendix A.1 we provide analytical expressions for the Fourier transforms of each of the weighting functions. In this step, we make one additional approximation beyond the erf approximation, which is to approximate w_0 as a linear combination of w_1 and w_2, which results from a power series approximation valid in the low-temperature limit, when $\Xi \ll \alpha$.

7.3   Results

For all of our simulations, we construct a Barker-Henderson hard sphere fluid with a diameter determined by Eq. 7.16 using the WCA potential as the pair potential. The BH fluid is known to give good results, so we use it as a reference for our DFT.

7.3.1   Homogeneous limit

As a simple test for the equation of state, we compare the theory for a homogeneous soft-sphere fluid to Monte Carlo simulation. The results shown in Figure 7.3 display very good agreement for lower densities across all temperatures shown in Figure and at higher temperatures which are not shown. Differences between the DFT
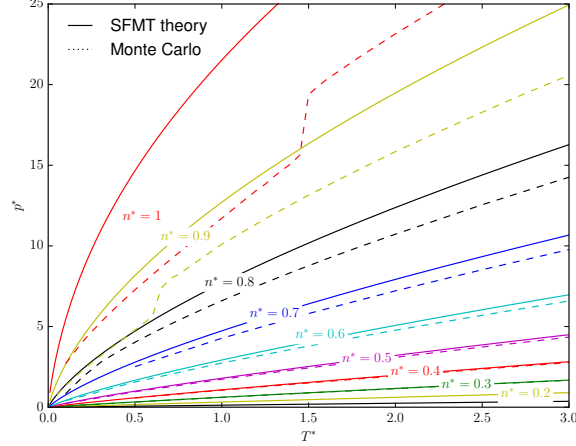
Figure 7.3: Reduced pressure versus temperature. The SFMT result is plotted as solid lines, with simulation results as dashed lines. The reduced pressure is defined in terms of the Lennard-Jones parameters as $p^* \equiv p\sigma^3/\epsilon$.

(solid lines) and MC results (dashed lines) become quite apparent at $n^* = 0.6$ and above, even at temperatures above the melting transition. Our theory consistently predicts higher pressures than simulations show, which is surprising given that Fig. 7.1 shows that the force should be *underestimated* by our theory at high packing.

For the remainder of our figures, we will focus on just two bulk reduced densities: 0.6 and 1.0. We have examined a wide variety of densities, and found that the agreement with simulation consistently improves as the density is decreased, and so we decided to focus on just these two interesting cases. At a reduced density of 0.6, our functional is right on the brink of its discrepancy with simulation, as is evident from Fig. 7.3. In contrast, the very high reduced density of 1.0 is well

beyond the point where our SFMT has considerably broken down quantitatively, and can demonstrate how it fails.

7.3.2   Soft spheres near a hard wall

To begin with the simplest test for inhomogeneous one dimensional behavior, we will look at the density profile for the soft sphere fluid near a hard wall. We note that a hard wall, in this context, is interpreted as a potential felt by our spheres that abruptly transitions from zero to infinity, in contrast to the hard wall felt by a rubber ball, which has a soft potential energy as the ball changes shape. Figure 7.4 shows the density profile for the WCA fluid near a hard wall. The top plot shows density profiles for $n^* = 0.6$ and the bottom for $n^* = 1.0$. We see that lower densities and higher temperatures produce almost exact results, while lower temperatures and higher densities reveal disagreement.

We find that the Barker-Henderson approach with the White Bear hard-sphere functional gives almost identical predictions to our method, with discrepancies between our SFMT and Barker-Henderson that are consistently much smaller than the error of either method relative to the Monte Carlo simulations.

7.3.3   Soft spheres near a soft wall

As a second and more physical case, we construct a wall of made of a continuum of WCA spheres with density ρ (see Chapter 8 for derivation). The potential at a
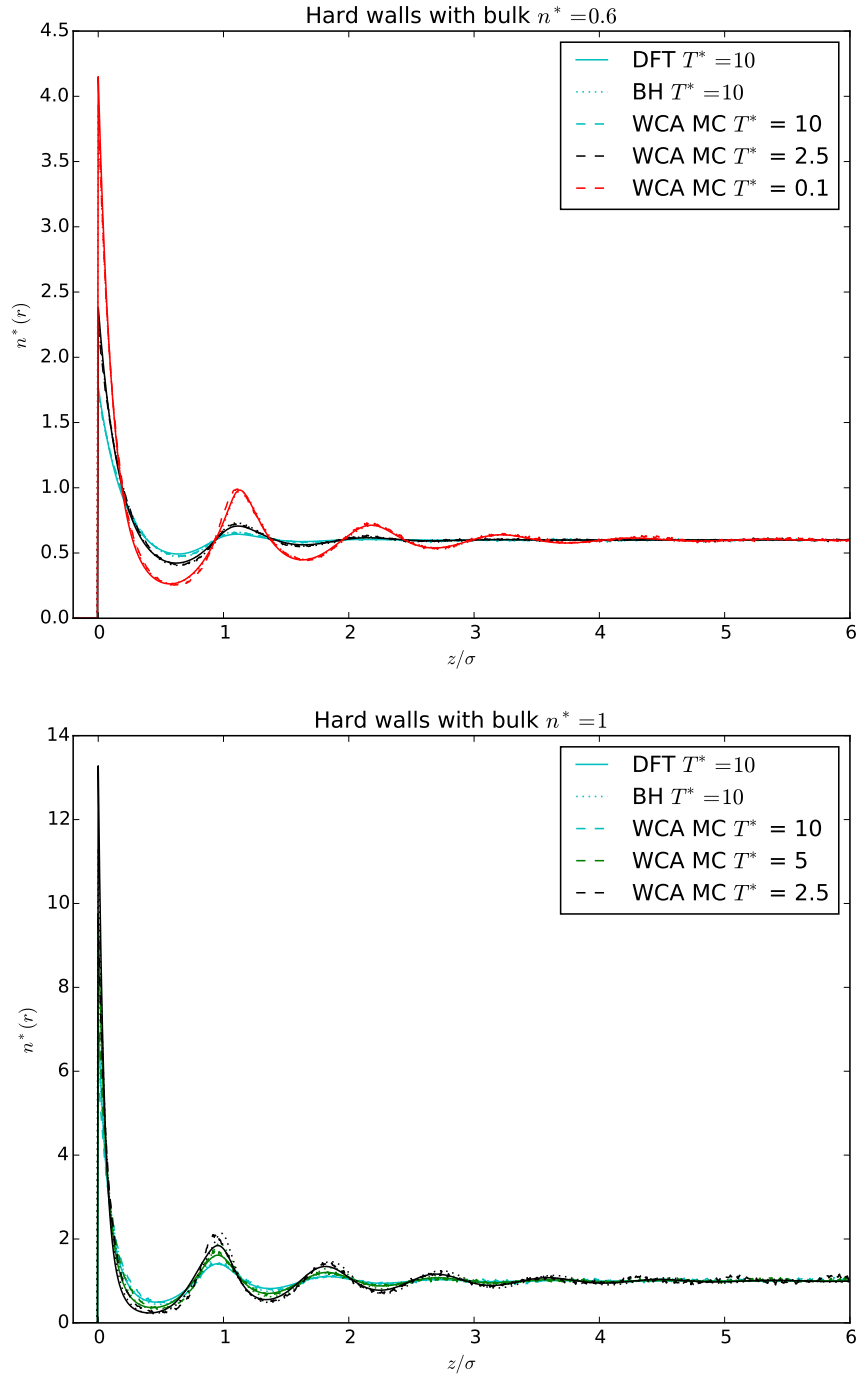
Figure 7.4: Density distribution of WCA fluid near a hard wall.
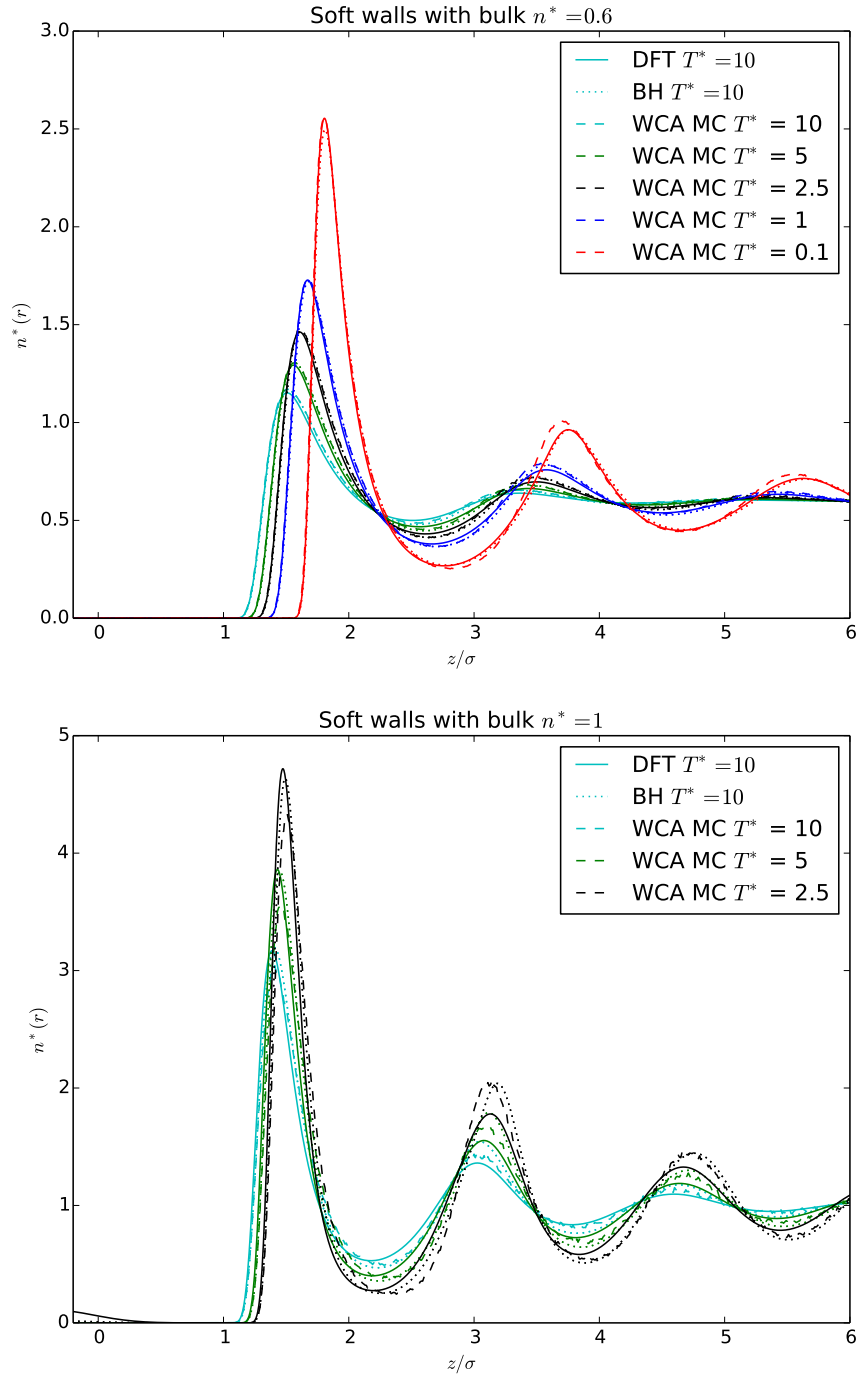
Figure 7.5: Density distribution of a WCA fluid near a soft wall.

distance z from such a wall is

$$V_{SW}(0 < z \le R_0) = 2\pi\rho\epsilon\left[\frac{2\sigma_W^{12}}{45}\left(\frac{1}{z^9} - \frac{1}{R_0^9}\right) + \frac{\sigma_W^6}{3}\left(\frac{1}{R_0^3} - \frac{1}{z^3}\right)\right.$$
$$\left. + \frac{z^3 - R_0^3}{6} + (R_0 - z)\left(\frac{R_0^2}{2} + \frac{\sigma_W^6}{R_0^4} - \frac{2\sigma_W^{12}}{5R_0^{10}}\right)\right]. \quad (7.25)$$

The distance R_0 is equal to a radius of a sphere which makes up the wall plus the radius of a sphere in the fluid. The potential is zero when $z > R_0$, and is infinite for $z \le 0$. Both ϵ and σ_W are Lennard-Jones parameters between the wall and the fluid. R_0 and σ_W are related by $\sigma_W = 2^{5/6}R_0$.

In Figure 7.5, we compare our soft sphere DFT against MC simulation and a BH fluid near a soft wall with the potential given in Equation 7.25. We plot the reduced density versus reduced distance from the surface of the wall for $n^* = 0.6$ at different temperatures. Again, the results of our soft sphere fluid is as good as the BH fluid overall.

7.3.4   Soft spheres radial distribution function

For three dimensional comparisons, we plot radial distribution functions computed using the test-particle approach. Results for reduced densities below $n^* = 0.6$ have been omitted as they were exact over temperature ranges from $T^* = 0.01$ to $T^* = 10$. The top frame of Fig. 7.6 (top) shows the radial distribution for a range of temperatures at a reduced density of $n^* = 0.6$. We see very good agreement of our DFT with Monte-Carlo simulation at this reduced density. Our DFT's behavior at
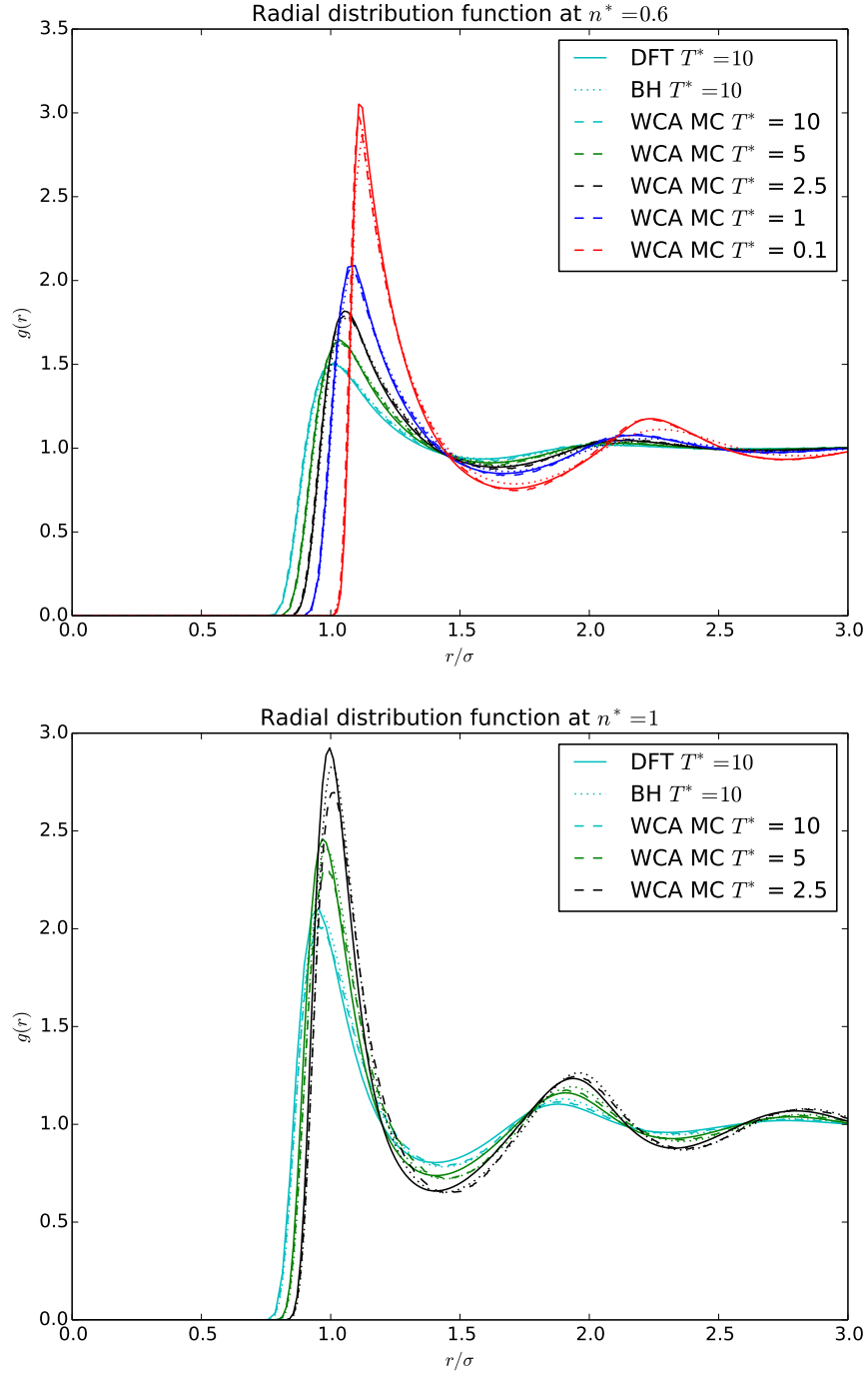
Figure 7.6: Radial distribution functions with 0.6 (top) and 1.0 (bottom) reduced densities. As in other figures, the solid lines give our SDFT result, the dashed lines give Monte Carlo simulation results, and the dotted line represents predictions using the Barker-Henderson approach.

higher temperatures are in almost exact agreement, while the lower temperatures have slight disagreement just after the first peak at contact and in the subsequent oscillations where it underestimates the amplitude of oscillation. Comparison with the Barker-Henderson results shows our DFT to have a similar magnitude of error relative the exact radial distribution function.

In Fig. 7.6 (bottom), we plot the results for a reduced density of $n^* = 1.0$ for three different temperatures. While both Barker-Henderson hard spheres and our DFT both overestimate the density at contact, our theory differs more at the lowest temperature shown here. For the density oscillations, our DFT's error is comparable to that of the Barker-Henderson results.

7.3.5 Argon

Finally, to connect with experiment, we model liquid the radial distribution function of Argon by computing the radial distribution of a WCA fluid surrounding a single Lennard-Jones particle. We consider three density/temperature pairs for which experimental data is available [92–94], and which roughly span the range of reduced densities from 0.6 to 1.0. The three experimental results were performed at vapor pressure, 9.92 MPa, and 1.1 GPa; and at temperatures of 85 K, 48 K, and 293 K respectively. For each system we compute the radial distribution function with Monte Carlo simulation, as well as SFMT and the Barker-Henderson approach. For our WCA fluid and Lennard-Jones test particle, we used the Lennard-Jones parameters developed by Verlet: $\sigma = 3.405$ Å and $\epsilon = 119.8$ K [95].
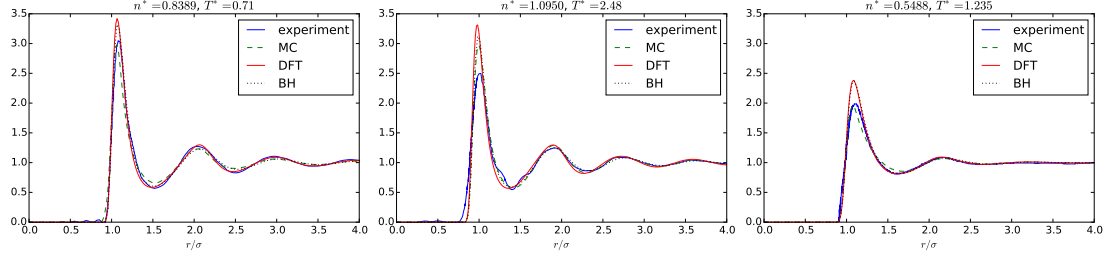
Figure 7.7: Radial distribution functions of Argon. From left to right the experimental data was taken at 85 K and vapor pressure, at 293 K and 1.1 GPa, and at 48 K and 9.92 MPa.

Figure 7.7 shows the resulting radial distribution functions. Our Monte Carlo data confirms that the WCA fluid can give a reasonably good prediction of the radial distribution function of a real liquid, albeit with some discrepancy in the first and second peak. Here the discrepancy between theory and simulation is somewhat larger, but again our new functional performs comparably to the Barker-Henderson approach. Both theories significantly overestimate the height of the first peak.

7.4 Conclusion

The theory presented in this paper is as good as a Barker-Henderson hard sphere fluid for a range of densities and temperatures. The advantage of our theory is that we can use it *as is* rather than needing to accommodate for discontinuities and delta functions of hard sphere fluids.

8 Soft wall potential derivation

This is the derivation for the Weeks-Chandler-Anderson (WCA) wall potential used for testing the soft sphere fluid in Chapter 7. We start with the WCA pair potential between two spheres:

$$
V_{WCA}(|\mathbf{r} - \mathbf{r'}|) = \begin{cases} 4\epsilon \left[\left(\frac{\sigma}{|\mathbf{r}-\mathbf{r'}|} \right)^{12} - \left(\frac{\sigma}{|\mathbf{r}-\mathbf{r'}|} \right)^{6} \right] + \epsilon & |\mathbf{r} - \mathbf{r'}| < R_0 \\ 0 & |\mathbf{r} - \mathbf{r'}| \geq R_0 \end{cases}
\tag{8.1}
$$

where R_0 is the addition of the radii of the two spheres. We construct a wall of WCA spheres by placing the centers of the spheres that make up the wall surface at $z = 0$ all along the x-y plane, and fill space from the plane to $z = -\infty$ with constant particle density ρ as shown in Figure 8.1. We then integrate on a test particle at $\mathbf{r}$ to find the total potential at that point due to all contributions from the wall,

$$
V_{SW}(\mathbf{r}) = \iiint \rho(\mathbf{r'}) V_{WCA}(|\mathbf{r} - \mathbf{r'}|) d\mathbf{r'}
\tag{8.2}
$$

Since we have an infinite plane at the wall surface, we can exploit symmetry by placing our test particle a distance z above the wall on the z-axis axis and integrating over cylindrical coordinates. This simplifies our center-to-center distance
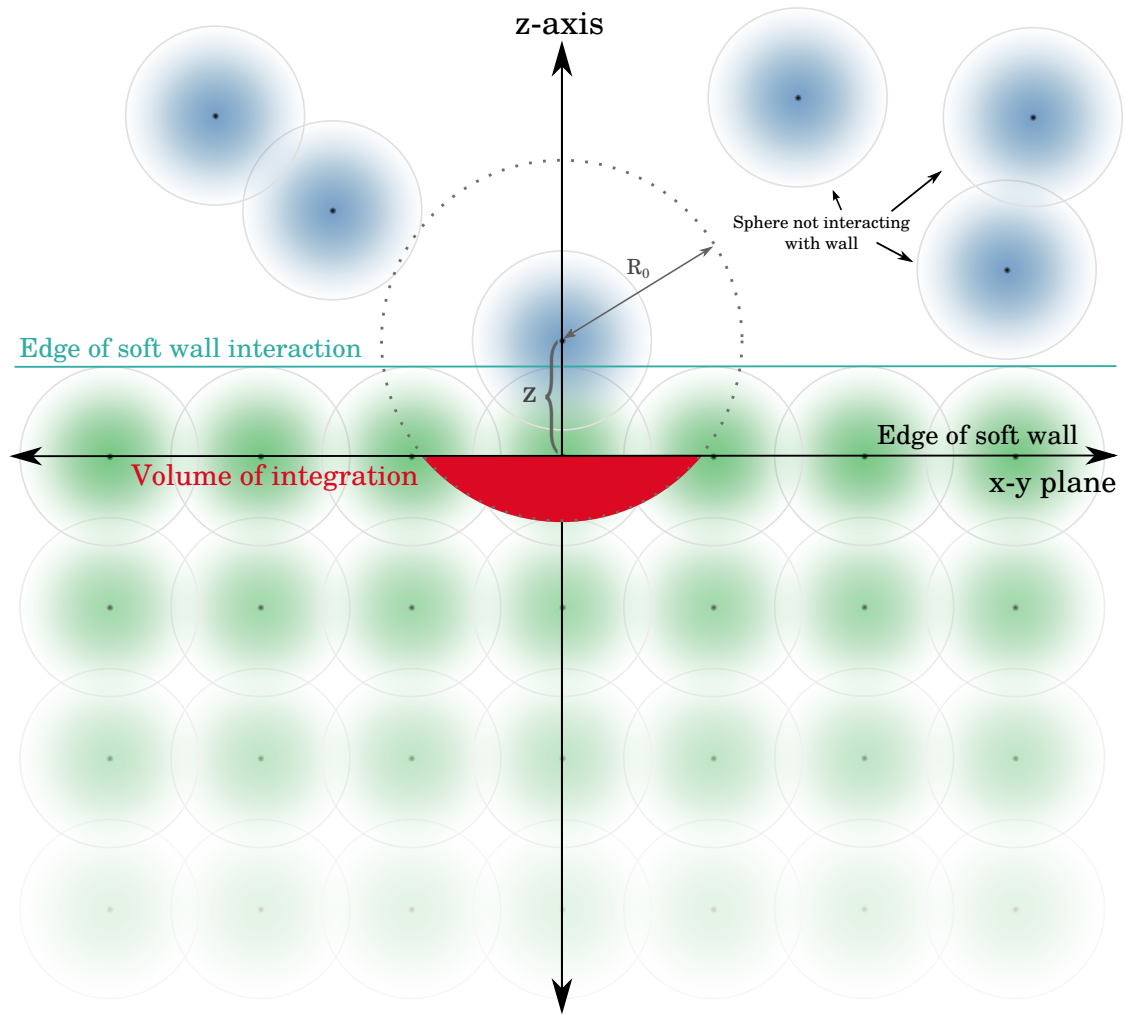
Figure 8.1: A visual diagram of the soft wall and the test particle. Green spheres make up the wall and blue spheres represent the fluid. The test particle has been placed on the z-axis to exploit symmetry in the integration. The x-y plane is located at the centers of the spheres that form the surface of the wall. z is the distance from that plane to the center of the test particle. The spheres that the wall is composed of are assumed to be much denser than shown here, and only those spheres whose centers are within the "Volume of integration" contribute.

to be

$$|\mathbf{r} - \mathbf{r}'| = \sqrt{r'^2 + (z - z')^2} \tag{8.3}$$

and allows the ϕ integration to simply become a factor of 2π. Since we must have $r'^2 + (z - z')^2 \leq R_0^2$, the limits in the $\hat{\mathbf{r}}$ direction go from zero to $\sqrt{R_0^2 - (z - z')^2}$. I'll save some space in the integration by calling this γ. Since the distance $z - z'$ can never be larger than R_0, the limits in the $\hat{\mathbf{z}}$ direction now go from $z - R_0$ to zero. This only applies as long as $z - z' \leq R_0$, otherwise the entire integral is zero. The following is the step-by-step integration of our function:

$$V_{SW} = 2\pi\rho\epsilon \int\limits_{z-R_0}^{0} \int\limits_{0}^{\gamma} \left(4 \left[\frac{\sigma_W^{12} r'}{\left(r'^2 + (z - z')^2 \right)^6} - \frac{\sigma_W^6 r'}{\left(r'^2 + (z - z')^2 \right)^3} \right] + r' \right) \mathrm{d}r' \mathrm{d}z' \tag{8.4}$$

$$= 2\pi\rho\epsilon \int\limits_{z-R_0}^{0} \left(\frac{-2\sigma_W^{12}}{5R_0^{10}} + \frac{\sigma_W^6}{R_0^4} + \frac{R_0^2 - (z - z')^2}{2} + \frac{2\sigma_W^{12}}{5(z - z')^{10}} - \frac{\sigma_W^6}{(z - z')^4} \right) \mathrm{d}z' \tag{8.5}$$

$$= 2\pi\rho\epsilon \left[\frac{z^3}{6} + \frac{2\sigma_W^{12}}{45z^9} - \frac{\sigma_W^6}{3z^3} - \frac{R_0^3}{6} - \frac{2\sigma_W^{12}}{45R_0^9} + \frac{\sigma_W^6}{3R_0^3} \right.$$

$$\left. - (z - R_0) \left(\frac{R_0^2}{2} + \frac{\sigma_W^6}{R_0^4} - \frac{2\sigma_W^{12}}{5R_0^{10}} \right) \right] \tag{8.6}$$

Now to clean this up a bit

$$V_{SW}(0 < z \leq R_0) = 2\pi\rho\epsilon \left[\frac{2\sigma_W^{12}}{45} \left(\frac{1}{z^9} - \frac{1}{R_0^9} \right) + \frac{\sigma_W^6}{3} \left(\frac{1}{R_0^3} - \frac{1}{z^3} \right) \right.$$
$$\left. + \frac{z^3 - R_0^3}{6} + (R_0 - z) \left(\frac{R_0^2}{2} + \frac{\sigma_W^6}{R_0^4} - \frac{2\sigma_W^{12}}{5R_0^{10}} \right) \right] \quad (8.7)$$

with $V_{SW} = 0$ when $z > R_0$ and $V_{SW} = \infty$ when $z \leq 0$.

9   Square well potential

9.1   Introduction

In Chapter 6 we tested an improvement for the association term of the free energy, and in Chapter 7 we focused on a theory that could effectively replace the hard sphere reference fluid in SAFT. In this chapter, I present a theory that would contribute to an improvement for the dispersive interaction and could thus be used in the dispersive free energy term, F_{disp}, in SAFT. This theory is in progress and exhibits less than ideal results. The purpose of this chapter is to present the theory, the current results, and suggest some possible solutions.

9.2   Theory

The square well fluid is not a novel fluid; it has been widely studied. This study differs by utilizing an approximation for the hard sphere pair distribution function at contact which was developed by our research group.
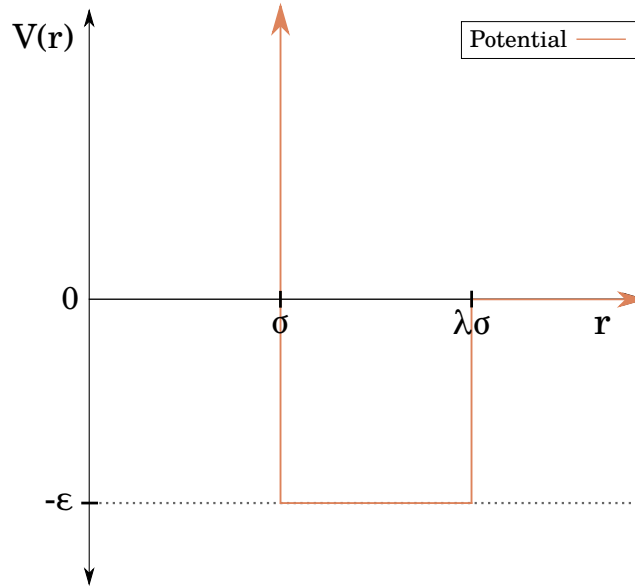
Figure 9.1: Graphical representation of the square well potential. σ is the hard sphere diameter, λ is the well width relative to σ, and ϵ well depth.

9.2.1 Square well potential

The pair potential that describes a square well is

$$V_{\text{SW}}(\mathbf{r}) = \begin{cases} \infty & r < \sigma \\ -\epsilon & \sigma < r < \lambda\sigma \\ 0 & \lambda\sigma < r \end{cases} \tag{9.1}$$

where ϵ is the depth of the attractive well, λ is the relative width of the well with respect to σ, and σ is twice the hard sphere radius. A visual representation of this potential is shown in Figure 9.1. One thing to note is that λ will be on the order

of 1, so this is a relatively long range interaction between hard spheres.

9.2.2 Perturbation

Since solutions to the hard sphere fluid are accurately known, we can treat this system with perturbation theory. In perturbation theory, the total potential for a given position is

$$v_\Lambda(\mathbf{r}) = v_{exact}(\mathbf{r}) + \Lambda w(\mathbf{r}) \tag{9.2}$$

where $v_{exact}(\mathbf{r})$ is potential for our reference system that we know exactly, $w(\mathbf{r})$ is our perturbative potential, and Λ is an dimensionless constant that gives us our "amount" of perturbation.

If we want to know the total potential of the whole system, we sum over all particle pairs:

$$V_N(\Lambda) = \sum_{ij} v_\Lambda(\mathbf{r}_{ij}) \tag{9.3}$$

9.2.3 Square well contribution in homogeneous case

The square well contribution to the free energy is based on thermodynamic perturbation theory (sometimes known as the "high temperature expansion"). We use a dispersion term based on the SAFT-VR approach [59], which has two parameters an interaction energy ϵ_d and a length scale $\lambda_d R$.

The SAFT-VR dispersion free energy has the form [59]

$$F_{\text{disp}}[n] = \int \left(a_1(\mathbf{r}) + \beta a_2(\mathbf{r})\right) n(\mathbf{r}) d\mathbf{r}, \tag{9.4}$$

where a_1 and a_2 are the first two terms in a high-temperature perturbation expansion and $\beta = 1/k_B T$. The first term, a_1, is the mean-field dispersion interaction. a_1 is given by

$$a_1(\mathbf{r}) = \int d\mathbf{r}' n(\mathbf{r}') g_{HS}^{(2)}(\mathbf{r}, \mathbf{r}') \Phi(|\mathbf{r} - \mathbf{r}'|) \tag{9.5}$$

where Φ is the pair potential, $g_{HS}^{(2)}$ is the two particle correlation function of the hard-sphere refernce fluid, and n is the single particle density. This expression looks almost like a convolution, which suggests working in Fourier space. For computational efficiency, we must Fourier transform this term over $\mathbf{r}$. Being that that only the $g_{HS}^{(2)}$ and Φ terms contain $\mathbf{r}$, we will only need to transform those terms together. The necessary transforms are shown in Section 9.2.5 below.

The second term, a_2, describes the effect of fluctuations resulting from compression of the fluid due to the dispersion interaction itself, and would be approximated using the local compressibility approximation (LCA), which assumes the energy fluctuation is simply related to the compressibility of a hard-sphere reference fluid [60]. Currently for this theory we don't use a_2, but it may be needed to fix disagreement we shall see in Figures 9.3 and 9.3.

9.2.4 The contact value approximation for the hard-sphere pair distribution function

Our research group recently introduced efficient an approximation for the pair distribution function of the inhomogeneous hard-sphere fluid [96]. This approximation takes the form:

$$g^{(2)}(\mathbf{r}_1, \mathbf{r}_2) = \frac{g_S(r_{12}, g_\sigma(\mathbf{r}_1)) + g_S(r_{12}, g_\sigma(\mathbf{r}_2))}{2} \qquad (9.6)$$

where $g_S(r, g_\sigma)$ is a separable fit to the radial distribution function of the homogeneous hard-sphere fluid, and $g_\sigma(\mathbf{r})$ is an approximation for the pair distribution function of an inhomogeneous hard-sphere fluid averaged over contact with a sphere located at position $\mathbf{r}$.

9.2.5 Polynomial expansion

We formulate g_S as a polynomial expansion up to fourth order so that

$$g_S(r; g_\sigma) = g_\sigma + \sum_i \gamma_i(g_\sigma)\xi_i(r) \qquad (9.7)$$

$$= g_\sigma + \sum_{i=1}^{4} \left(\sum_{j=1}^{4} (g_\sigma - 1)^j \kappa_{ji} \right) \left(\frac{r}{\sigma} - 1 \right)^i, \qquad (9.8)$$

where, to be clear about γ_i and ξ_i

$$\gamma_i(g_\sigma) = \left(\sum_{j=1}^{4} (g_\sigma - 1)^j \kappa_{ji} \right) \tag{9.9}$$

$$\xi_i = \left(\frac{r}{\sigma} - 1 \right)^i. \tag{9.10}$$

To turn this into usable code for computation, we need to perform a Fourier transform on $g_s(r, g_\sigma)v_{SW}(\mathbf{r})$,

$$\tilde{g}_s(k, g_\sigma) = \iiint g_s(r, g_\sigma) u_{SW}(\mathbf{r}) e^{-i\mathbf{k}\cdot\mathbf{r}} d^3\mathbf{r} \tag{9.11}$$

With only radial dependence in g_s, the Fourier transform becomes

$$\tilde{g}_s(k, g_\sigma) = \frac{4\pi}{k} \int_0^\infty \left(g_\sigma + \sum_i \gamma_i \xi_i(r) \right) \Phi(r) r \sin(kr) dr \tag{9.12}$$

$$= -\epsilon \frac{4\pi}{k} \int_\sigma^{\lambda\sigma} \left(g_\sigma + \sum_i \gamma_i \xi_i(r) \right) r \sin(kr) dr. \tag{9.13}$$

For the g_σ term, we treat it like a "zeroth" term where $\xi_0(r) = 1$, so that we're only transforming the potential well multiplied by g_σ. Fourier transforms of each term are shown below starting from the g_σ term then the i terms in numerical order.

$$\frac{4\pi}{k} \int_\sigma^{\lambda\sigma} g_\sigma r \sin(kr) dr = \frac{4\pi g_\sigma}{k} \int_\sigma^{\lambda\sigma} r \sin(kr) dr$$

$$= \frac{4\pi g_\sigma}{k^3} \left[\sin(k\lambda\sigma) - k\lambda\sigma \cos(k\lambda\sigma) - \sin(k\sigma) + k\sigma \cos(k\sigma) \right] \tag{9.14}$$

$$\frac{4\pi}{k} \int_\sigma^{\lambda\sigma} \gamma_1 \xi_1 r \sin(kr) \mathrm{d}r = \frac{4\pi\gamma_1}{k} \int_\sigma^{\lambda\sigma} \left(\frac{r}{\sigma} - 1\right) r \sin(kr) \mathrm{d}r$$

$$= \frac{4\pi\gamma_1}{k^4\sigma} \left[\left\{2 - \lambda k^2 \sigma^2 (\lambda - 1)\right\} \cos(k\lambda\sigma) - 2\cos(k\sigma) \right.$$

$$\left. - k\sigma \left\{ \sin(k\sigma) + (1 - 2\lambda)\sin(k\lambda\sigma) \right\} \right] \quad (9.15)$$

$$\frac{4\pi}{k} \int_\sigma^{\lambda\sigma} \gamma_2 \xi_2 r \sin(kr) \mathrm{d}r = \frac{4\pi\gamma_2}{k} \int_\sigma^{\lambda\sigma} \left(\frac{r}{\sigma} - 1\right)^2 r \sin(kr) \mathrm{d}r$$

$$= \frac{4\pi\gamma_2}{k^5\sigma^2} \left[\left\{k^2\sigma^2(1 - 4\lambda + 3\lambda^2) - 6\right\} \sin(k\lambda\sigma) \right.$$

$$- k\sigma \left\{4 + \lambda(k^2\sigma^2(\lambda - 1)^2 - 6)\right\} \cos(k\lambda\sigma)$$

$$\left. + 6\sin(k\sigma) - 2k\sigma\cos(k\sigma) \right] \quad (9.16)$$

$$\frac{4\pi}{k} \int_\sigma^{\lambda\sigma} \gamma_3 \xi_3 r \sin(kr) \mathrm{d}r = \frac{4\pi\gamma_3}{k} \int_\sigma^{\lambda\sigma} \left(\frac{r}{\sigma} - 1\right)^3 r \sin(kr) \mathrm{d}r$$

$$= \frac{4\pi\gamma_3}{k^6\sigma^3} \left[k\sigma \left\{6\sin(k\sigma) + (18 - 24\lambda + k^2\sigma^2(\lambda - 1)^2(4\lambda - 1))\sin(k\lambda\sigma)\right\} \right.$$

$$+ \left\{6k^2\sigma^2(\lambda - 1)(2\lambda - 1) - \lambda k^4\sigma^4(\lambda - 1)^3 - 24\right\} \cos(k\lambda\sigma)$$

$$\left. + 24\cos(k\sigma) \right] \quad (9.17)$$

Figure 9.2: Radial distribution function for a filling fraction of 0.2, $\epsilon = 1$, $\sigma = 1$, and $\lambda = 1.3$ for three temperatures. The dotted lines are Monte-Carlo simulation and the solid lines are theory. The general shape is correct, but we do see significant differences.

$$\frac{4\pi}{k} \int_{\sigma}^{\lambda\sigma} \gamma_4 \xi_4 r \sin(kr) \mathrm{d}r = \frac{4\pi\gamma_4}{k} \int_{\sigma}^{\lambda\sigma} \left(\frac{r}{\sigma} - 1\right)^4 r \sin(kr) \mathrm{d}r$$

$$= \frac{4\pi\gamma_4}{k^7\sigma^4} \left[\left\{ k^2\sigma^2(\lambda - 1)(36 - 60\lambda + k^2\sigma^2(\lambda - 1)^2(5\lambda - 1)) + 120 \right\} \sin(k\lambda\sigma) \right.$$

$$+ k\sigma \left\{ 24\cos(k\sigma) - (24(5\lambda - 4) - 4k^2\sigma^2(\lambda - 1)^2(5\lambda - 2) \right.$$

$$\left. \left. + \lambda k^4\sigma^4(\lambda - 1)^4)\cos(k\lambda\sigma) \right\} - 120\sin(k\sigma) \right] \quad (9.18)$$
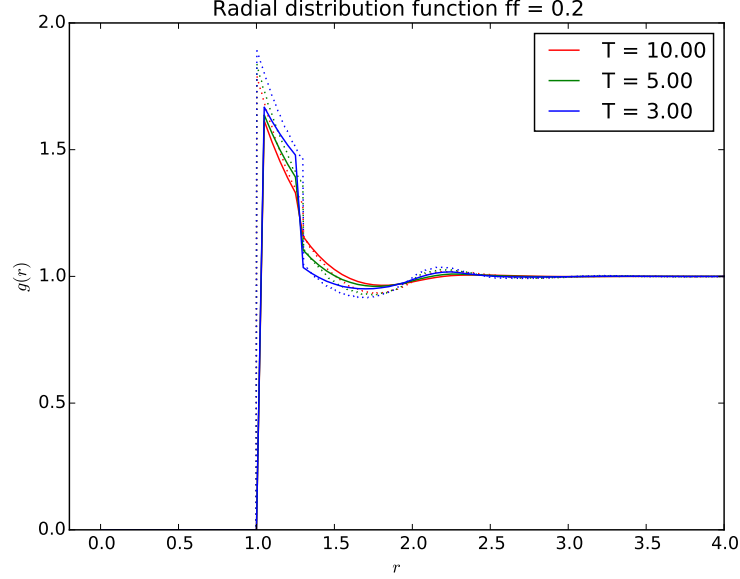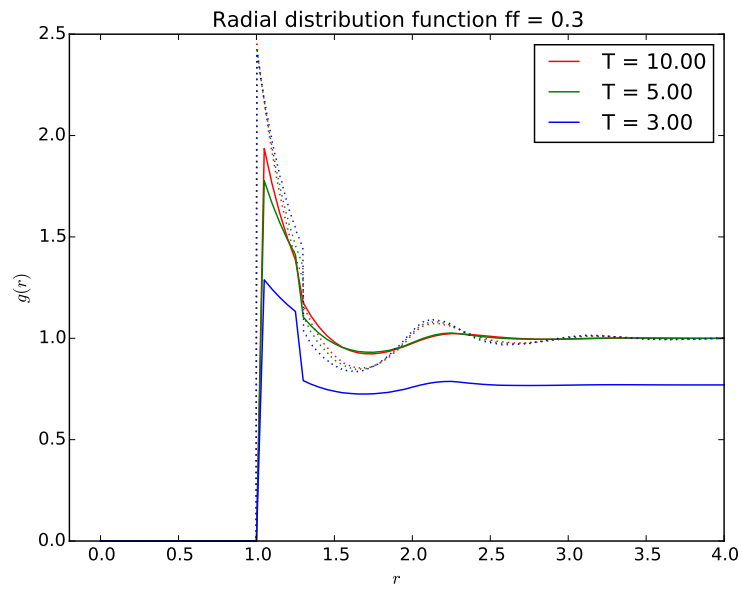
Figure 9.3: Radial distribution function for a filling fraction of 0.3, $\epsilon = 1$, $\sigma = 1$, and $\lambda = 1.3$ for three temperatures. The dotted lines are Monte-Carlo simulation and the solid lines are theory. The general shape is correct, but we do see significant differences.

9.3 Homogeneous fluid results

We simulate the radial distribution function of a homogeneous square well fluid with filling fractions 0.2 and 0.3 using the theory described, using the test-particle approach, in which we simulate a fluid in an external potential representing a single particle. We use the same hard sphere diameter, well depth ϵ, well width λ, and temperatures for both simulations. We compare the radial distribution function $g(r)$ against against Monte-Carlo simulation in Figures 9.2 and 9.3.

It can be seen that although the general shape of the radial distribution is the same, there are significant deviations in the g at contact, and the behaviors of the oscillations just after the well stops. In Fig 9.3 it is apparent that the lower temperature result gives the wrong bulk filling fraction. These less than satisfactory result leads us to believe that we may need to include a_2 in our theory, or there is a mistake made either in the derivation or the code.

9.4 Conclusion

This theory currently produces results which are qualitatively similar to Monte-Carlo simulation, but lack of strong agreement and breakdown at lower temperatures will need to be addressed. Specifically, the behavior at lower temperatures approaching liquid suggest a problem in the bulk limit.

10 Conclusion

In this dissertation I have discussed motivations for studying water, introduced statistical associating fluid theory (SAFT), and presented a background of classical density function theory (cDFT) including fundamental measure theory. I began with a cDFT for water based on an existing SAFT model. I followed this with three attempts to improve individual terms in the SAFT free energy. First, we applied an improved correlation function at contact to address issues with the association term. Secondly, I have displayed my work on a soft sphere fluid theory based on soft fundamental measure theory, which could provide an improved reference system replacing that of hard spheres. This theory produces results that are as good as Barker-Henderson hard spheres over a wide range of densities and temperatures but does not require the extra care needed to handle the step and delta functions that arise in the density functional theory of hard spheres. Furthermore, the soft sphere fluid is more physical for almost all liquids. Finally, I have discussed my progress towards an improved theory for the inhomogeneous square well fluid, which will require more consideration before it is tractable.

APPENDIX

A   Weighting functions in Fourier space for soft sphere fluid

A.1   Weighting functions in Fourier space

We Fourier transform our weight functions to perform simulations in Fourier space. We find that

$$\tilde{w}_3(k) = \frac{4\pi}{k} \int_0^\infty r w_3(r) \sin(kr) dr \tag{A.1}$$

$$= \frac{4\sqrt{\pi}}{k^3} \int_{-\sigma/2a}^\infty \left[\sin(k(au + \frac{\sigma}{2})) - k(au + \frac{\sigma}{2}) \cos(k(au + \frac{\sigma}{2})) \right] e^{-u^2} du. \tag{A.2}$$

This is not an analytic function, but we assume that we are working at low enough temperatures so that our function reduces to zero by $u = -\frac{\sigma}{2a}$. We extend the

lower limit to $-\infty$ then

$$\tilde{w}_3(k) \approx \frac{4\pi}{k^3}e^{-\left(\frac{ak}{2}\right)^2}\left[\left(1 + \frac{a^2k^2}{2}\right)\sin\left(\frac{k\sigma}{2}\right) - \frac{k}{2}\sigma\cos\left(\frac{k\sigma}{2}\right)\right] \qquad (A.3)$$

We apply the same method to the other weight functions and find that:

$$\tilde{w}_2(k) = \frac{2\pi}{k}e^{-\left(\frac{ak}{2}\right)^2}\left(a^2k\cos\left(\frac{k\sigma}{2}\right) + \sigma\sin\left(\frac{k\sigma}{2}\right)\right) \qquad (A.4)$$

$$\tilde{w}_1(k) = \frac{1}{k}e^{-\left(\frac{ak}{2}\right)^2}\sin\left(\frac{k\sigma}{2}\right) \qquad (A.5)$$

$$\tilde{\mathbf{w}}_{2V}(\mathbf{k}) = \frac{i\pi}{k}e^{-\left(\frac{ak}{2}\right)^2}\left[\left(\sigma^2 - a^4k^2\right)\cos\left(\frac{k\sigma}{2}\right) - 2\sigma\left(a^2k + \frac{1}{k}\right)\sin\left(\frac{k\sigma}{2}\right)\right]\hat{\mathbf{k}}$$

$$(A.6)$$

$$\tilde{\mathbf{w}}_{1V}(k) = \frac{i}{k}e^{-\left(\frac{ak}{2}\right)^2}\left[\frac{\sigma}{2}\cos\left(\frac{k\sigma}{2}\right) - \left(\frac{a^2k}{2} + \frac{1}{k}\right)\sin\left(\frac{k\sigma}{2}\right)\right]\hat{\mathbf{k}}, \qquad (A.7)$$

$\tilde{w}_0(k)$ contains a $\frac{1}{r}$ term in its integrand that can be expanded as an infinite series. The first two terms were kept and could be expressed in terms of $\tilde{w}_1(k)$ and $\tilde{w}_2(k)$.

$$\tilde{w}_0(k) = \frac{2}{\sigma}\left[2\tilde{w}_1(k) - \frac{1}{2\pi\sigma}\tilde{w}_2(k)\right] \qquad (A.8)$$

This results in another approximation we must make. In real space we modify n_0 to agree with Equation A.8. So

$$n_0(\mathbf{r}) \approx \frac{2}{\alpha}\left[2n_1(\mathbf{r}) - \frac{1}{2\pi\alpha}n_2(\mathbf{r})\right] \qquad (A.9)$$

Bibliography

[1] Water Structure and Science webpage by Martin Chaplin. http://www1.lsbu.ac.uk/water/water_structure_science.html. Under "The Phase Diagram of water" section (http://www1.lsbu.ac.uk/water/water_phase_diagram.html, retrieved August 16, 2015).

[2] E. W. Lemmon, M. O. McLinden, and D. G. Friend. *NIST Chemistry WebBook, NIST Standard Reference Database Number 69*, chapter Thermophysical Properties of Fluid Systems. National Institute of Standards and Technology, Gaithersburg MD, 20899, 2010. http://webbook.nist.gov, (retrieved December 15, 2010).

[3] D.M. Huang, P.L. Geissler, and D. Chandler. Scaling of hydrophobic solvation free energies. *Journal of Physical Chemistry B*, 105(28):6704–6709, 2001.

[4] Jessica Hughes, Eric J Krebs, David Roundy, et al. A classical density-functional theory for describing water interfaces. *The Journal of chemical physics*, 138(2):024509–024509, 2013.

[5] Daniel T Bowron, Adriano Filipponi, Mark A Roberts, and John L Finney. Hydrophobic hydration and the formation of a clathrate hydrate. *Physical review letters*, 81(19):4164, 1998.

[6] T. Lewis, B. Winter, A. C. Stern, M. D. Baer, C. J. Mundy, D. J. Tobias, and J. C. Hemminger. *J. Phys. Chem. C*, 115(43):21183–21190, 2011.

[7] S. Yoo, X.C. Zeng, and S.S. Xantheas. On the phase diagram of water with density functional theory potentials: The melting temperature of ice i with the perdew–burke–ernzerhof and becke–lee–yang–parr functionals. *The Journal of chemical physics*, 130:221102, 2009.

[8] S. Yoo and S.S. Xantheas. Communication: The effect of dispersion corrections on the melting temperature of liquid water. *The Journal of chemical physics*, 134:121105, 2011.

[9] M. S. Wertheim. Fluids with highly directional attractive forces. i. statistical thermodynamics. *Journal of statistical physics*, 35(1):19–34, 1984.

[10] M. S. Wertheim. Fluids with highly directional attractive forces. ii. thermodynamic perturbation theory and integral equations. *Journal of statistical physics*, 35(1):35–47, 1984.

[11] M. S. Wertheim. Fluids with highly directional attractive forces. iii. multiple attraction sites. *Journal of statistical physics*, 42(3):459–476, 1986.

[12] M. S. Wertheim. Fluids with highly directional attractive forces. iv. equilibrium polymerization. *Journal of statistical physics*, 42(3):477–492, 1986.

[13] Yaakov Rosenfeld. Free-energy model for the inhomogeneous hard-sphere fluid mixture and density-functional theory of freezing. *Phys. Rev. Lett.*, 63(9):980–983, Aug 1989.

[14] P. Hohenberg and W. Kohn. Inhomogeneous electron gas. *Physical Review*, 136(3B):B864, 1964.

[15] N.D. Mermin. Thermal properties of the inhomogeneous electron gas. *Physical Review*, 137(5A):1441–1443, 1965.

[16] C. Ebner, WF Saam, and D. Stroud. Density-functional theory of simple classical fluids. i. surfaces. *Physical Review A*, 14(6):2264, 1976.

[17] R. Car and M. Parrinello. Unified approach for molecular dynamics and density-functional theory. *Phys. Rev. Lett.*, 55(22):2471–2474, Nov 1985.

[18] Jeffrey C. Grossman, Eric Schwegler, Erik W. Draeger, Francois Gygi, and Giulia Galli. Towards an assessment of the accuracy of density functional theory for first principles simulations of water. *The Journal of Chemical Physics*, 120(1):300–311, 2004.

[19] I.C. Lin, A.P. Seitsonen, M.D. Coutinho-Neto, I. Tavernelli, and U. Rothlisberger. Importance of van der waals interactions in liquid water. *The Journal of Physical Chemistry B*, 113(4):1127–1131, 2009.

[20] J. Wang, G. Roma´ n Pe´ rez, J.M. Soler, E. Artacho, and MV Ferna´ ndez Serra. Density, structure, and dynamics of water: The effect of van der waals interactions. *Journal of Chemical Physics*, 134(2):24516, 2011.

[21] A. Møgelhøj, A.K. Kelkkanen, K.T. Wikfeldt, J. Schiøtz, J.J. Mortensen, L.G.M. Pettersson, B.I. Lundqvist, K.W. Jacobsen, A. Nilsson, and J.K. Nørskov. Ab initio van der waals interactions in simulations of water alter structure from mainly tetrahedral to high-density-like. *The Journal of Physical Chemistry B*, 115(48):14149–14160, 2011.

[22] R. Jonchiere, A.P. Seitsonen, G. Ferlat, A.M. Saitta, and R. Vuilleumier. Van der waals effects in ab initio water at ambient and supercritical conditions. *The Journal of chemical physics*, 135:154503, 2011.

[23] J.A. Morrone and R. Car. Nuclear quantum effects in water. *Physical review letters*, 101(1):17801, 2008.

[24] K. Lum, D. Chandler, and J.D. Weeks. Hydrophobicity at small and large length scales. *The Journal of Physical Chemistry B*, 103(22):4570–4577, 1999.

[25] Wendell M. Latimer, Kenneth S. Pitzer, and Cyril M. Slansky. The free energy of hydration of gaseous ions, and the absolute potential of the normal calomel electrode. *The Journal of Chemical Physics*, 7(2):108–111, 1939.

[26] Alexander A. Rashin and Barry Honig. Reevaluation of the born model of ion hydration. *Journal of Physical Chemistry*, 89(26):5588–5593, 1985.

[27] Chang-Guo Zhan, John Bentley, and Daniel M. Chipman. Volume polarization in reaction field theory. *J. Chem. Phys.*, 108(1):177–192, 1998.

[28] Chao-Ping Hsu, Martin Head-Gordon, and Teresa Head-Gordon. Reaction field cavity optimization: A born-again born model for ionic hydration. *J. Chem. Phys.*, 111(21):9700–9704, December 1999.

[29] A. Hildebrandt, R. Blossey, S. Rjasanow, O. Kohlbacher, and H.-P. Lenhof. Novel formulation of nonlocal electrostatics. *Physical Review Letters*, 93(10):108104, 2004.

[30] Andreas Hildebrandt, Ralf Blossey, Sergej Rjasanow, Oliver Kohlbacher, and Hans-Peter Lenhof. Electrostatic potentials of proteins in water: a structured continuum approach. *Bioinformatics*, 23(2):e99–103, 2007.

[31] W. A. Curtin and N. W. Ashcroft. Weighted-density-functional theory of inhomogeneous liquids and the freezing transition. *Phys. Rev. A*, 32(5):2909–2919, Nov 1985.

[32] Yaakov Rosenfeld. Free energy model for inhomogeneous fluid mixtures: Yukawa-charged hard spheres, general interactions, and plasmas. *J. Chem. Phys.*, 98(10):8126–8148, May 1993.

[33] Y. Rosenfeld, M. Schmidt, H. Löwen, and P. Tarazona. Fundamental-measure free-energy density functional for hard spheres: Dimensional crossover and freezing. *Phys. Rev. E*, 55(4):4245–4263, Apr 1997.

[34] P. Tarazona and Y. Rosenfeld. From zero-dimension cavities to free-energy functionals for hard disks and hard spheres. *Phys. Rev. E*, 55(5):R4873–R4876, May 1997.

[35] P. Tarazona. Density functional for hard sphere crystals: A fundamental measure approach. *Phys. Rev. Lett.*, 84(4):694–697, Jan 2000.

[36] R. Roth, R. Evans, A. Lang, and G. Kahl. Fundamental measure theory for hard-sphere mixtures revisited: the White Bear version. *Journal of Physics: Condensed Matter*, 14:12063, 2002.

[37] Y.X. Yu and J. Wu. Structures of hard-sphere fluids from a modified fundamental-measure theory. *The Journal of chemical physics*, 117:10156, 2002.

[38] Kejian Ding, David Chandler, S. J. Smithline, and A. D. J. Haymet. Density-functional theory for the freezing of water. *Phys. Rev. Lett.*, 59(15):1698–1701, Oct 1987.

[39] B. Yang, D.E. Sullivan, B. Tjipto-Margo, and C.G. Gray. Density-functional theory of the water liquid-vapour interface. *Molecular Physics*, 76(3):709–735, June 1992.

[40] B. Yang, DE Sullivan, and CG Gray. Density-functional theory of the water liquid-vapour interface: Ii. *Journal of Physics: Condensed Matter*, 6:4823, 1994.

[41] G.J. Gloor, F.J. Blas, E.M. del Rio, E. de Miguel, and G. Jackson. A saft-dft approach for the vapour-liquid interface of associating fluids. *Fluid phase equilibria*, 194:521–530, 2002.

[42] G.J. Gloor, G. Jackson, F.J. Blas, E.M. Del Río, and E. de Miguel. An accurate density functional theory for the vapor-liquid interface of associating

chain molecules based on the statistical associating fluid theory for potentials of variable range. *The Journal of chemical physics*, 121:12740, 2004.

[43] G.J. Gloor, G. Jackson, FJ Blas, E.M. del Río, and E. de Miguel. Prediction of the vapor-liquid interfacial tension of nonassociating and associating fluids with the saft-vr density functional theory. *The Journal of Physical Chemistry C*, 111(43):15513–15522, 2007.

[44] Khuloud Jaqaman, Kagan Tuncay, and Peter J. Ortoleva. Classical density functional theory of orientational order at interfaces: Application to water. *J. Chem. Phys.*, 120(2):926–938, 2004.

[45] Gary NI Clark, Andrew J Haslam, Amparo Galindo, and George Jackson. Developing optimal wertheim-like models of water for use in statistical associating fluid theory (saft) and related approaches. *Molecular physics*, 104(22-24):3561–3581, 2006.

[46] G. N. Chuev and V. F. Sokolov. Hydration of hydrophobic solutes treated by the fundamental measure approach. *Journal of Physical Chemistry B*, 110(37):18496–18503, 2006.

[47] J. Lischner and TA Arias. Classical density-functional theory of inhomogeneous water including explicit molecular structure and nonlinear dielectric response. *The Journal of Physical Chemistry B*, 114(5):1946–1953, 2010.

[48] D. Fu and J. Wu. Vapor- Liquid Equilibria and Interfacial Tensions of Associating Fluids within a Density Functional Theory. *Ind. Eng. Chem. Res*, 44(5):1120–1128, 2005.

[49] SB Kiselev and JF Ely. A new analytical formulation for the generalized corresponding states model for thermodynamic and surface properties in pure fluids. *Chemical Engineering Science*, 61(15):5107–5113, 2006.

[50] F.J. Blas, E.M. Del Río, E. De Miguel, and G. Jackson. An examination of the vapour-liquid interface of associating fluids using a saft-dft approach. *Molecular Physics*, 99(22):1851–1865, 2001.

[51] R. Sundararaman, K. Letchworth-Weaver, and T. A. Arias. A computationally efficacious free-energy functional for studies of inhomogeneous liquid water. *The Journal of chemical physics*, 137(4):044107–1–044107–6, 2012.

[52] CHAD J. Segura, WALTER G. Chapman, and KESHAWA P. SHUKLA. Associating fluids with four bonding sites against a hard wall: density functional theory. *Molecular Physics*, 90(5):759–772, 1997.

[53] C.J. Segura, E.V. Vakarin, W.G. Chapman, and MF Holovko. A comparison of density functional and integral equation theories vs monte carlo simulations for hard sphere associating fluids near a hard wall. *The Journal of chemical physics*, 108(12):4837–4848, 1998.

[54] Y.X. Yu and J. Wu. A fundamental-measure theory for inhomogeneous associating fluids. *The Journal of Chemical Physics*, 116:7094, 2002.

[55] E. A. Müller and K. E. Gubbins. Molecular-based equations of state for associating fluids: A review of saft and related approaches. *Industrial & engineering chemistry research*, 40(10):2193–2211, 2001.

[56] J. Gross. A density functional theory for vapor-liquid interfaces using the pcp-saft equation of state. *The Journal of chemical physics*, 131:204705, 2009.

[57] H. Kahl and J. Winkelmann. Modified pt-lj-saft density functional theory:: I. prediction of surface properties and phase equilibria of non-associating fluids. *Fluid Phase Equilibria*, 270(1-2):50–61, 2008.

[58] W.G. Chapman, K.E. Gubbins, G. Jackson, and M. Radosz. Saft: equation-of-state solution model for associating fluids. *Fluid Phase Equilibria*, 52:31–38, 1989.

[59] A. Gil-Villegas, A. Galindo, P.J. Whitehead, S.J. Mills, G. Jackson, and A.N. Burgess. Statistical associating fluid theory for chain molecules with attractive potentials of variable range. *The Journal of Chemical Physics*, 106:4168, 1997.

[60] J.A. Barker and D. Henderson. What is "liquid"? understanding the states of matter. *Reviews of Modern Physics*, 48(4):587, 1976.

[61] J.H. Walther, R.L. Jaffe, EM Kotsalis, T. Werder, T. Halicioglu, and P. Koumoutsakos. Hydrophobic hydration of c¡ sub¿ 60¡/sub¿ and carbon nanotubes in water. *Carbon*, 42(5):1185–1194, 2004.

[62] F. Sedlmeier, D. Horinek, and R.R. Netz. Entropy and enthalpy convergence of hydrophobic solvation beyond the hard-sphere limit. *The Journal of chemical physics*, 134:055105, 2011.

[63] C. Vega and E. De Miguel. Surface tension of the most popular models of water by using the test-area simulation method. *The Journal of chemical physics*, 126:154707, 2007.

[64] Eric J Krebs, Jeff B Schulte, and David Roundy. Improved association in a classical density functional theory for water. *The Journal of chemical physics*, 140(12):124507, 2014.

[65] Jeff B Schulte, Patrick A Kreitzberg, Chris V Haglund, and David Roundy. Using fundamental measure theory to treat the correlation function of the inhomogeneous hard-sphere fluid. *Physical Review E*, 86(6):061201, 2012.

[66] Guillaume Jeanmairet, Maximilien Levesque, Rodolphe Vuilleumier, and Daniel Borgis. Molecular density functional theory of water. *The Journal of Physical Chemistry Letters*, 4(4):619–624, 2013.

[67] Shuangliang Zhao, Rosa Ramirez, Rodolphe Vuilleumier, and Daniel Borgis. Molecular density functional theory of solvation: From polar solvents to water. *The Journal of chemical physics*, 134:194102, 2011.

[68] Shuangliang Zhao, Zhehui Jin, and Jianzhong Wu. New theoretical method for rapid prediction of solvation free energy in water. *The Journal of Physical Chemistry B*, 115(21):6971–6975, 2011.

[69] Rosa Ramirez, Michel Mareschal, and Daniel Borgis. Direct correlation functions and the density functional theory of polar solvents. *Chemical physics*, 319(1):261–272, 2005.

[70] Rosa Ramirez and Daniel Borgis. Density functional theory of solvation and its relation to implicit solvent models. *The Journal of Physical Chemistry B*, 109(14):6754–6763, 2005.

[71] Maximilien Levesque, Virginie Marry, Benjamin Rotenberg, Guillaume Jeanmairet, Rodolphe Vuilleumier, and Daniel Borgis. Solvation of complex surfaces via molecular density functional theory. *The Journal of chemical physics*, 137:224107, 2012.

[72] Maximilien Levesque, Rodolphe Vuilleumier, and Daniel Borgis. Scalar fundamental measure theory for hard spheres in three dimensions: Application to hydrophobic solvation. *The Journal of Chemical Physics*, 137:034115, 2012.

[73] Sugata P Tan, Hertanto Adidharma, and Maciej Radosz. Recent advances and applications of statistical associating fluid theory. *Industrial & Engineering Chemistry Research*, 47(21):8063–8082, 2008.

[74] David Chandler. Interfaces and the driving force of hydrophobic assembly. *Nature*, 437:640–647, 2005.

[75] Dietmar Paschek. Temperature dependence of the hydrophobic hydration and interaction of simple solutes: An examination of five popular water models. *The Journal of chemical physics*, 120:6674, 2004.

[76] MA Lucretius. De rerum natura, 60 BCE.

[77] JS Rowlinson. The statistical mechanics of systems with steep intermolecular potentials. *Molecular Physics*, 8(2):107–115, 1964.

[78] John A Barker and Douglas Henderson. Perturbation theory and equation of state for fluids. ii. a successful theory of liquids. *The Journal of Chemical Physics*, 47(11):4714–4721, 1967.

[79] Hans C Andersen, John D Weeks, and David Chandler. Relationship between the hard-sphere fluid and fluids with realistic repulsive forces. *Physical Review A*, 4(4):1597, 1971.

[80] Thomas Lafitte, Anastasia Apostolakou, Carlos Avendaño, Amparo Galindo, Claire S Adjiman, Erich A Müller, and George Jackson. Accurate statistical associating fluid theory for chain molecules formed from mie segments. *The Journal of chemical physics*, 139(15):154504, 2013.

[81] Norman F Carnahan and Kenneth E Starling. Equation of state for nonattracting rigid spheres. *The Journal of Chemical Physics*, 51(2):635–636, 1969.

[82] José A Cuesta and Yuri Martínez-Ratón. Dimensional crossover of the fundamental-measure functional for parallel hard cubes. *Physical review letters*, 78(19):3681, 1997.

[83] Hendrik Hansen-Goos and Klaus Mecke. Fundamental measure theory for inhomogeneous fluids of nonspherical hard particles. *Physical Review Letters*, 102(1):018302, 2009.

[84] Matthieu Marechal and Hartmut Löwen. Density functional theory for hard polyhedra. *Physical review letters*, 110(13):137801, 2013.

[85] Matthias Schmidt. Density-functional theory for soft interactions by dimensional crossover. *Physical Review E*, 60(6):R6291, 1999.

[86] Matthias Schmidt. Density functional for additive mixtures. *Physical Review E*, 62(3):3799, 2000.

[87] Benito Groh and Matthias Schmidt. Density-functional theory for structure and freezing of star polymer solutions. *The Journal of Chemical Physics*, 114(12):5450–5456, 2001.

[88] Soon-Chul Kim. Adsorption of a polydisperse soft-sphere fluid in a slit pore. *The Journal of Chemical Physics*, 114(21):9593–9598, 2001.

[89] MB Sweatman. Fundamental measure theory for pure systems with soft, spherically repulsive interactions. *Journal of Physics: Condensed Matter*, 14(46):11921, 2002.

[90] M. Schmidt. Fluid structure from density-functional theory. *Physical Review E*, 62(4):4976–4981, 2000.

[91] John D. Weeks, David Chandler, and Hans C. Andersen. Role of repulsive forces in determining the equilibrium structure of simple liquids. *The Journal of Chemical Physics*, 54(12):5237–5247, 1971.

[92] PG Mikolaj and CJ Pings. Structure of liquids. iii. an x-ray diffraction study of fluid argon. *The Journal of Chemical Physics*, 46(4):1401–1411, 2004.

[93] Jon H Eggert, Gunnar Weck, Paul Loubeyre, and Mohamed Mezouar. Quantitative structure factor and density measurements of high-pressure fluids in diamond anvil cells by x-ray diffraction: Argon and water. *Physical Review B*, 65(17):174105, 2002.

[94] JL Yarnell, MJ Katz, Ro Go Wenzel, and SH Koenig. Structure factor and radial distribution function for liquid argon at 85 k. *Physical Review A*, 7(6):2130, 1973.

[95] Loup Verlet. Computer" experiments" on classical fluids. i. thermodynamical properties of lennard-jones molecules. *Physical review*, 159(1):98, 1967.

[96] Paho Lurie-Gregg, Jeff B Schulte, and David Roundy. Approach to approximating the pair distribution function of inhomogeneous hard-sphere fluids. *Physical Review E*, 90(4):042130, 2014.